Title: Sex regulated gene dosage effect of PPARα on synaptic plasticity.

Authors: Nathalie Pierrot[1,2*], Laurence Ris[3], Ilie-Cosmin Stancu[1,2,4], Anna Doshina[1,2], Floriane Ribeiro[1,2], Donatienne Tyteca[1,5], Eric Baugé[6], Fanny Lalloyer[6], Liza Malong[1,2], Olivier Schakman[1,2], Karelle Leroy[7], Pascal Kienlen-Campard[1,2], Philippe Gailly[1,2], Jean-Pierre Brion[7], Ilse Dewachter[1,2,4], Bart Staels[6] and Jean-Noël Octave[1,2].

Affiliations:

[1] Université catholique de Louvain, B-1200 Brussels, Belgium,

[2] Institute of Neuroscience, B-1200 Brussels, Belgium,

[3] Laboratory of Neuroscience, Health Institute, University of Mons, B-7000, Mons, Belgium,

[4] Biomedical Research Institute, Hasselt University, 3500 Hasselt, Belgium.

[5] de Duve Institute, B-1200 Brussels, Belgium

[6] Université de Lille EGID, Inserm, CHU Lille, Institut Pasteur de Lille, U1011, F-59000 Lille, France.

[7] Laboratory of Histology and Neuropathology, Université libre de Bruxelles, 1070 Brussels, Belgium.

* Corresponding author: Nathalie Pierrot, Université catholique de Louvain, Institute of Neuroscience, Alzheimer Dementia, avenue Mounier 53, SSS/IONS/CEMO-Bte B1.53.03, B-1200, Brussels, Belgium. Office: +32 2 764 93 34

E-mail: nathalie.pierrot@uclouvain.be

Running Title: PPARα and synaptic plasticity

Keywords: AMPAR, GluA1, LTP, NMDAR, PPARα, synaptic plasticity.

Summary blurb: Differences in PPARα expression between males and females affects the regulation of GluA1 expression and synaptic plasticity in mice.

Abstract

Mechanisms driving cognitive improvements following nuclear receptors activation are poorly understood. The peroxisome proliferator-activated nuclear receptor alpha (PPARα) forms heterodimers with the nuclear retinoid X receptor (RXR). We report that PPARα mediates the improvement of hippocampal synaptic plasticity upon RXR activation in a transgenic mouse model with cognitive deficits. This improvement results from an increase in GluA1 subunit expression of the alpha-amino-3-hydroxy-5-methyl-4-isoxazolepropionic acid (AMPA) receptor, eliciting an AMPA response at the excitatory synapses. Associated with a two times higher PPARα expression in males than in females, we show that male, but not female, PPARα null mutants display impaired hippocampal long-term potentiation. Moreover, PPARα-knockdown in the hippocampus of cognition-impaired mice compromises the beneficial effects of RXR activation on synaptic plasticity only in males. Furthermore, selective PPARα activation with pemafibrate improves synaptic plasticity in male cognition-impaired mice, but not in females. We conclude that striking sex differences in hippocampal synaptic plasticity are observed in mice, related to differences in PPARα expression levels.

Introduction

The nuclear receptor (NR) superfamily of ligand-dependent transcription factors are broadly implicated in a wide variety of biological processes regulating energy balance, inflammation, lipid and glucose metabolism (Evans & Mangelsdorf, 2014). NRs play an important role in the adaptive responses to environmental changes by controlling directly the expression of target genes through binding to sequence-specific elements located in gene regulatory regions (Evans & Mangelsdorf, 2014). Among NRs, peroxisome proliferator-activated receptors (PPAR) and the liver X receptors (LXR) form obligate heterodimers with retinoid X receptors (RXR). PPAR/RXR and LXR/RXR heterodimers are permissive, meaning that receptor dimers can be activated by ligands for either partner in the dimer, or even by both synergistically (Evans & Mangelsdorf, 2014).

PPARs, including PPARα, PPARβ/δ and PPARγ, are master metabolic regulators in response to dietary changes. PPARα plays an important role in the regulation of fatty acid catabolism (Staels et al, 1998). LXRs isoforms (LXRα and LXRβ) are involved in lipogenesis and reverse cholesterol transport (Bensinger & Tontonoz, 2008). Furthermore, PPARs and LXRs have also anti-inflammatory effects since they repress transcription of genes encoding pro-inflammatory cytokines (reviewed in (Bensinger & Tontonoz, 2008)).

These nuclear receptors are abundantly expressed in metabolically active tissues, including the brain of rodents and humans (Warden et al, 2016). Due to their anti-inflammatory and potential neuroprotective effects, PPARs, LXRs and RXRs activation with specific agonists emerged as promising approaches for treating brain pathologies in several mouse models of Parkinson, Huntington, Alzheimer diseases, multiple and amyotrophic lateral sclerosis, stroke

and even in a mouse model with physiological brain aging-dependent cognitive decline (reviewed in (Moutinho & Landreth, 2017; Zolezzi et al, 2017)).

Recent data indicate that activation of RXRs (Mariani et al, 2017) or PPARs (Roy et al, 2013) upregulates the expression of a set of synaptic-related proteins involved in excitatory neurotransmission. Moreover, RXR activation increases dendritic complexity and branching of neurons promoting their differentiation and development (Mounier et al, 2015; Nam et al, 2016). However, the link between NRs activation and the improvement of synaptic plasticity is missing.

In the present work, we analyzed how RXR activation improves synaptic plasticity and neuronal function and identified PPARα as a crucial player. Upon RXR activation, the PPARα-dependent upregulation of GluA1 subunit-containing AMPA receptors mediates long-term potentiation (LTP) improvement in transgenic mice and AMPA responses in cortical cells. Associated with a higher expression of PPARα in males than in females, the absence of PPARα severely impairs LTP and GluA1 expression only in males. Knockdown of PPARα in the hippocampus of cognition-impaired mice abrogates the beneficial effects of RXR activation only in males. In these mice, treatment with pemafibrate, a highly potent selective PPARα activator (Hennuyer et al, 2016; Yamazaki et al, 2007), improves synaptic plasticity only in males, demonstrating a key role of PPARα in the regulation of synaptic function in a sex specific manner.

Results

Synaptic plasticity, AMPA responses and GluA1 expression are improved upon RXR activation

We first assessed *in vivo* the effect of RXR activation on synaptic plasticity in a well-characterized transgenic (Tg) mouse model of Alzheimer's disease (5xFAD), in which age-dependent synaptic and cognitive deficits occur (Oakley et al, 2006). We measured LTP in the hippocampal CA3-CA1 synapses, which is defined as an activity-dependent enhancement of synaptic strength involved in memory processing (Bliss & Collingridge, 1993). Impaired LTP found in Tg 5xFAD hippocampus was recovered ($P<0.0001$) after oral administration of bexarotene for 12 days and became similar to vehicle treated control mice (Fig 1A). Bexarotene did not improve LTP of Wt mice (Fig S1A). The efficiency of the treatment of Tg mice could result from a breakdown of the blood-brain barrier in 5XFAD mice (Montagne et al, 2017). This recovery of LTP in 5xFAD mice was observed together with improved cognition in the object recognition and spatial navigation tasks, which was independent of amyloid plaque load in different regions of the brain (Figs S1B-1E).

We next analyzed whether the RXR activation-mediated improvement of LTP was related to changes in expression levels of N-methyl-D-aspartate receptors (NMDARs) and AMPA receptors (AMPARs), known to be required for LTP at the excitatory synapses (Bliss & Collingridge, 1993). We therefore measured expression of both GluN2A-, GluN2B-containing NMDARs and GluA1-containing AMPARs in hippocampal lysates of these mice. While GluN2A ($P=0.0070$), 2B ($P=0.0019$) and GluA1 ($P=0.0007$) decreased in Tg mice compared to Wt mice, a 12 days treatment of Tg mice with the RXR agonist bexarotene specifically increased GluA1-containing AMPARs ($P=0.0379$) (Fig 1B). These results indicate that improvement in

synaptic plasticity by RXR activation is tightly associated with an increased expression of GluA1 subunit in treated Tg animals.

The RXR activation-mediated GluA1 increase described above could have an impact on basal glutamatergic responses. Rat cortical cells in culture were treated or not with bexarotene (100 nM) for 24h, and NMDARs and AMPARs subunits measured. At 13-14 days *in vitro* (DIV), GluN2A (P=0.0655) and 2B (P=0.2916) were unchanged by bexarotene treatment (Fig 1C). In contrast, GluA1 protein was increased (P=0.0003) in these cells treated with bexarotene (Fig 1C). Increase in GluA1 protein level was also observed in hippocampal neurons (P=0.0133) and in 7 DIV (P=0.0273) cultured hippocampal slices incubated with a higher bexarotene concentration of 300 nM (Figs S2A and 2B).

Since activation of AMPA and NMDA receptors mediates Ca^{2+} entry into cells, we monitored AMPA and NMDA-induced Ca^{2+} responses in cortical cell cultures with the Fura-2 AM Ca^{2+}-sensitive dye by using single-cell calcium imaging. Measurements of fluorescence intensity changes showed that only AMPA (P<0.0001) (but not NMDA, P>0.9999) elicited a stronger Ca^{2+} increase with a larger amplitude in bexarotene-treated than in control cortical cells (Fig 1D). The higher Ca^{2+} permeability of GluA1-containing AMPARs observed in bexarotene-treated cortical cells did not result from changes in GluA2 expression, a subunit known to modify AMPARs properties by forming heteromeric complexes with GluA1 (reviewed in (Derkach et al, 2007)) (Fig S2C).

To address whether RXR-activation induces membrane insertion of GluA1-containing AMPARs, we quantified GluA1 expressed at the cell surface following biotinylation of cell surface proteins in cortical cells treated or not with bexarotene. Activation of RXR increased GluA1 protein levels in both the total (P=0.0002) and biotinylated (P=0.0273) fraction as compared to control

(Fig 1E). We next tested the influence of bexarotene treatment on the synaptic localization of GluA1-containing AMPARs, by measuring their co-localization with SynGAP, a Ras-GTPase activating protein highly enriched at excitatory synapses (Chen et al, 1998). GluA1 fluorescence intensity was higher and exhibited a more punctuated pattern in bexarotene treated cells compared to control (Figs. 1F and 1G). When post-synaptic puncta were quantified, GluA1-containing AMPARs were increased by bexarotene compared to control (Fig 1H) and exhibited a stronger overlap with the SynGAP postsynaptic marker after bexarotene treatment (Fig 1H**)**. Concomitantly, a decrease in the number of SynGAP peaks by bexarotene was observed compared to control (Fig 1H). In addition, a significant twofold increase in the average cluster size of GluA1 puncta (P<0.0001) was observed when comparing treated with control cells (Fig 1I). Together, these results support the hypothesis that RXR activation improves AMPA responses by increasing GluA1 expression and its targeting to the excitatory synapses.

PPARα is necessary for RXR activation-mediated improvements

Next, we investigated the cellular mechanisms by which RXR activation increases the expression of the GluA1 containing AMPARs. We first analyzed whether the expression of the cAMP response element binding (CREB) protein, involved in the synaptic maintenance of GluA1 subunit (Middei et al, 2013), was responsive to RXR activation (Nam et al, 2016). Both GluA1 (P=0.0486) and CREB mRNA (P=0.0007) as well as CREB protein (P=0.0006) levels and immunostaining intensity were increased in bexarotene treated cortical cells compared to control (Figs S3A and 3B).

Since RXR forms dimeric complexes with other NRs and that autoregulation and cross regulation of NRs have been described (Lefebvre et al, 2010; Tata, 1994), we wondered whether

the bexarotene-mediated RXR activation could modulate expression levels of the most prominent NRs found as obligate permissive heterodimers with RXR in neuronal and non-neuronal cells (reviewed in (Bookout et al, 2006; Zolezzi et al, 2017)). We did not observe any modification in mRNA levels of RXRα ($P>0.9999$), β ($P=0.8478$), γ ($P>0.9999$), PPARβ ($P=0.2070$), PPARγ ($P=0.3110$), and LXRβ ($P=0.6481$) isoforms in cortical cells treated with bexarotene (Fig 2A). In contrast, we observed a two fold increase in PPARα ($P=0.0005$) mRNA levels (Fig 2A) together with an increased immunostaining of PPARα in bexarotene treated cortical cells compared to control (Fig S3C). These results indicate that bexarotene-mediated RXR activation specifically increases PPARα expression.

We next analyzed whether upregulation of GluA1 expression by RXR activation depends on PPARα expression. We first measured GluA1 expression in cultured cortical cells from wild type (*Wt*) and PPARα deficient (*Ppara*$^{-/-}$) mice (Figs S4A and 4B). As expected (Roy et al, 2013), absence of PPARα decreased GluA1 expression at mRNA ($P=0.0079$) and protein ($P<0.0001$) levels in cortical cells (Figs S4C and 4D). In addition, the lower GluA1 expression in *Ppara*$^{-/-}$ cells was consistent with a decreased AMPA-induced Ca^{2+} response ($P<0.0001$) in these cells (Fig S4E). A PPAR-responsive-element was recently identified in the *Creb* promoter identifying it as a PPARα target (Roy et al, 2013), and we show that CREB mRNA ($P=0.0079$) levels are decreased in *Ppara*$^{-/-}$ cells (Fig S4C).

To address whether the RXR activation-mediated GluA1 upregulation could be PPARα dependent, *Wt* and *Ppara*$^{-/-}$ cultured cortical cells were treated or not with bexarotene. PPARα deficiency totally prevented the increase in GluA1 mRNA and protein levels ($P=0.6385$ and $P=0.1801$) observed in *Wt* cells treated with bexarotene (Figs 2B, 2C and 2D). On the contrary, the expression of ATP-binding cassette transporter A1 (ABCA1), a membrane protein driving

cholesterol efflux (Venkateswaran et al, 2000), known to be regulated by LXR upon RXR activation, was still increased by bexarotene in *Ppara*$^{-/-}$ cortical cells (P<0.0001, Fig 2B and P=0.0023, Fig 2D). This clearly demonstrates that GluA1 but not ABCA1 expression is regulated by the RXR/PPARα heterodimer.

Measurements of fluorescence intensity changes showed that AMPA elicited a greater Ca^{2+} increase with a larger amplitude only in *Wt* (P<0.0001) but not in *Ppara*$^{-/-}$ (P>0.9999) cells treated with bexarotene (Figs 2E and 2F). Thus, increased expression of the GluA1 subunit of AMPARs by activation of RXR is PPARα dependent.

PPARα deficiency impairs LTP and GluA1 expression in male mice

PPARα is required for normal cognitive function (D'Agostino et al, 2015; Roy et al, 2013). As previously reported (Dotson et al, 2016), PPARα mRNA levels (P<0.0001) are higher in the hippocampus of male than female mice (Fig 3A) prompting us to study potential sex different responses. Surprisingly, LTP induced by a single tetanus was significantly larger (P<0.0001) in 5-6 months old males than in females (Fig 3B). Interestingly, GluA1 mRNA (P=0.0021) and protein (P=0.0058) expression levels were higher in *Wt* male than female mice (Figs 3C and 3D), although similar GluN2A and 2B mRNA and protein levels were measured in males and females (Figs 3C and 3D).

Absence of PPARα expression in 5-6 months old *Ppara*$^{-/-}$ female mice did not influence either the potentiation induced by one train of stimulation or its maintenance as compared to *Wt* mice (Figs 3B and 3E). In contrast, both induction and maintenance of LTP were strongly reduced in *Ppara*$^{-/-}$ male mice compared to *Wt* mice (Figs 3B and 3E). A specific decreased expression of GluA1 was measured at the mRNA (P=0.0012) and protein (P=0.0003) level in *Ppara*$^{-/-}$ male

mice but not in females (Figs. 3F and 3G). Taken together these results suggest that PPARα induces sex-dependent modifications in LTP by specifically affecting the expression of the GluA1 subunit of AMPARs only in male mice.

Synaptic plasticity improved by RXR activation is PPARα and sex dependent

We next wondered whether the improved synaptic plasticity and GluA1 expression observed in bexarotene treated Tg animals (5xFAD mice) are mediated by PPARα. Since disruption of PPARα decreases lifespan in 5xFAD mice (Corbett et al, 2015), we decided to acutely decrease PPARα expression in the hippocampus of 9-10 months old Tg mice by using a serotype 9 adeno-associated viruses coding a shRNA construct designed to target endogenous PPARα (AAV-ShPpara). A scrambled ShRNA (AAV-ShSc) was used as control. We first tested the efficiency of AAV-ShPpara construct *in vitro* following transduction of cultured cortical cells at 4 DIV. Ten days after transduction, PPARα immunoreactivity was significantly decreased (P=0.0152) in AAV-ShPpara compared to AAV-ShSc transduced cells (Fig S5A). Neuronal activity measured by spontaneous calcium oscillations and amplitude of AMPA-induced Ca^{2+} responses were reduced (P<0.0001) in AAV-ShPpara compared to AAV-ShSc infected cells (Figs S5B and 5C, respectively). PPARα knockdown, while not affecting ABCA1 expression (P>0.9999), decreased GluA1 mRNA (P=0.0005) and protein (P<0.0001) levels by about 50 % (Fig S5D). In addition, PPARα knockdown abolished the increase in GluA1 mRNA and protein levels (P=0.6051 and P=0.1655, respectively) observed in AAV-ShSc cells treated with bexarotene (100 nM, 24h) (Figs S6A and 6B). On the contrary, ABCA1 mRNA and protein expression were still induced in AAV-ShSc (P=0.0058 and P<0.0001, respectively) and -ShPpara (P=0.0052 and P<0.0001, respectively) cortical cells treated with bexarotene (Figs S6A and 6B). Measurement

of fluorescence intensity changes showed that AMPA elicited a greater Ca^{2+} increase (P<0.0001) with a larger amplitude only in AAV-ShSc but not in AAV-ShPpara (P>0.9999) transduced cells treated with bexarotene (Figs S6C and 6D).

We next analyzed *in vivo* the effect of the acute knockdown of PPARα expression after stereotaxic injection of AAV-ShPpara and -ShSc constructs in the right and left hippocampi of Tg mice, respectively (Fig 4A). Since PPARα and GluA1 expression differ between males and females, the effect of knockdown of PPARα was studied in males and females separately. PPARα (P=0.0019) and GluA1 (P=0.0103) mRNA as well as GluA1 (P=0.0021) protein levels were higher in males compared to females (Figs S7A and 7B). Three weeks after stereotaxic AAV injection, PPARα mRNA levels (P=0.0001) significantly decreased in the hippocampi of male Tg mice injected with AAV-ShPpara to levels similar (P=0.7796) to those detected in female Tg mice injected with AAV-ShSc (Fig 4B). A significant but less pronounced decrease in PPARα mRNA (P=0.0239) was also observed in female Tg mice injected with AAV-ShPpara (Fig 4B), an effect likely due to the lower baseline PPARα expression in female mice (Fig 4B). In association with this difference in PPARα expression between males and females, PPARα knockdown decreased GluA1 protein levels (P=0.0028) only in hippocampal lysates from male Tg mice injected with AAV-ShPpara but not in females (P=0.1894) (Figs 4C and 4D). GluN2A and 2B protein expression was not affected by the treatment (Figs 4C and 4D). Next, we wondered whether PPARα was needed for the recovery of synaptic plasticity induced by RXR activation. We first measured LTP on hippocampal slices from male Tg mice treated or not for 2.5 h with bexarotene 4 µM (Fig S7C). The results were similar to those obtained following gavage of Tg mice. LTP was then measured on hippocampal slices from male and female Tg mice injected with AAV-ShPpara or -ShSc and incubated with bexarotene 4 µM. After 2.5 h of

bexarotene incubation, the potentiation induced by high frequency stimulation was lower in male Tg male mice injected with AAV-ShPpara compared to those injected with AAV-ShSc (Fig 4E). Moreover, LTP progressively decreased (P<0.0001) in male Tg mice injected with AAV-ShPpara compared to male Tg mice injected with AAV-ShSc three hours after the train of stimulation (Fig 4E). Both induction and maintenance of LTP were not affected in female Tg mice injected with AAV-ShPpara compared to AAV-ShSc (Fig 4F). Taken together these results show that improvement of synaptic plasticity by RXR activation is PPARα and sex dependent.

Sex specific improvement of LTP by pemafibrate

We then tested the effect of direct activation of PPARα using pemafibrate, a selective agonist for PPARα (Hennuyer et al, 2016; Yamazaki et al, 2007). We first assessed *in vivo* the effectiveness of PPARα activation in 12 months old male and female Tg (5xFAD) mice treated for 12 days by oral gavage with pemafibrate (Hennuyer et al, 2016) or vehicle. As previously described in human hepatocytes and mouse liver (Raza-Iqbal et al, 2015), we observed an increase in mRNA levels of PDK4 (P=0.0049), a PPARα target gene, in hippocampal lysates from Tg mice treated with pemafibrate (Fig S8A). These results demonstrate that oral administration of pemafibrate is able to activate PPARα in the brain.

We then measured the effect of pemafibrate on LTP. Although PPARα (P=0.0070), PPARβ (P=0.0348) and PPARγ (P=0.0083) mRNA levels were lower in Tg compared to *Wt* mice (Fig S8B), the decreased LTP observed in male Tg mice treated with vehicle was nevertheless recovered (P<0.0001) following treatment with pemafibrate (Fig 5A). Both induction and maintenance of LTP were strongly improved in male Tg mice with pemafibrate compared to vehicle (Fig 5A). However, activation of PPARα in female Tg mice did not influence LTP

potentiation nor its maintenance compared to vehicle (Fig 5B). In male Tg mice treated with pemafibrate, mRNA and protein levels of the GluN2A (P=0.0037 and P=0.0214, respectively) and GluA1 (P=0.0276 and P=0.0453) subunits were significantly upregulated compared to male Tg mice treated with vehicle (Figs 5C and 5D, respectively). No significant increase in the NMDARs and AMPARs subunits was measured in pemafibrate compared to vehicle treated female Tg mice (Figs 5E and 5F). Taken together, these results show that activation of PPARα with pemafibrate improves synaptic plasticity in a sex specific manner with a pharmacological response (increase in both GluN2A and GluA1 expression) different from that resulting from RXR activation (increase in GluA1 expression).

Discussion

We report here that PPARα, a master metabolic regulator involved in fatty acid catabolism (Staels et al, 1998), plays a central role in hippocampal synaptic plasticity by driving the expression of the GluA1 subunit of AMPARs in a sex specific manner.

We show that LTP improvement observed in a Tg mouse model of Alzheimer's disease (AD) upon RXR activation with bexarotene is concomitant with the specific upregulation of GluA1 expression. Adult GluA1 knockout mice cannot generate LTP and have cognitive abnormalities (Schmitt et al, 2005), indicating that the GluA1 subunit plays a critical role in synaptic plasticity and cognition. Even in the absence of any modification in NMDARs subunits, we cannot rule out that changes in subunits composition or posttranslational modifications that affect NMDARs gating and trafficking and also AMPARs function (for review see (Derkach et al, 2007)), could occur following RXR activation.

In cortical cells in culture, we show that RXR activation with bexarotene induces a cell-autonomous increase in the expression of the GluA1 subunit. We show that GluA1 upregulation induced by RXR activation was totally abolished in absence of PPARα whereas the expression of the LXR target gene, *ABCA1*, was still induced. Therefore, RXR/LXR activation increases *ABCA1* gene transcription, while RXR/PPARα activation drives the upregulation of GluA1 expression (Fig 6A).

Due to differences in expression levels of PPARα between males and females (Dotson et al, 2016), a sex difference in the regulation of GluA1 expression and synaptic plasticity by PPARα was found (Fig 6B). Many different pathways, which do not involve PPARα, can control GluA1 expression, and we cannot conclude that LTP difference between WT males and females relies only on a differential expression of PPARα. Nevertheless, a two times higher expression of

PPARα in males than in females induces a PPARα-mediated regulation of GluA1 expression only in males. This suggests that a threshold level of PPARα expression is needed to regulate GluA1 expression, and this level is not reached in females, which are insensitive to bexarotene treatment. Hormones are known to influence the expression of PPARα in a sex specific manner since gonadectomy of male rats decreases PPARα expression levels (Jalouli et al, 2003). Estrogens are known to improve synaptic plasticity and behavior is affected in ovariectomized female rats (reviewed in (Arevalo et al, 2015)).

Consistent with the central role of PPARα in fatty acid (FA) catabolism (Staels et al, 1998), PPARα null mice exhibit greater lipid accumulation (Chung et al, 2018). PPARα gene expression levels dose-dependently control liver metabolism, inflammation and atherogenesis (Lalloyer et al, 2011) and are tightly regulated by cellular content in FA. Low plasma free FA increases PPARα mRNA level in human skeletal muscle (Watt et al, 2004), whereas lipid accumulation decreases PPARα expression in the renal tubular epithelial region in rats (Chung et al, 2018), suggesting that the availability of FA is important for the regulation of *Ppara* gene transcription. Accumulation of FA has been previously reported in female but not male mice carrying FAD mutations (Barrier et al, 2010). Such FA accumulation could explain why PPARα expression is lower in female 5xFAD Tg mice.

Fibrates are PPARα agonists used in the treatment of hypertriglyceridemia, mixed dyslipidemia and also prevent the progression of atherosclerotic lesions (reviewed in (Gross et al, 2017)). Fenofibrate has been widely utilized, but its relatively low activity on PPARα led to the development of pemafibrate, a more potent and selective agonist for PPARα (Hennuyer et al, 2016; Yamazaki et al, 2007). In recent clinical studies, pemafibrate improved lipid profiles in patients with type 2 diabetes and hypertriglyceridemia (Araki et al, 2018) with a much higher

efficacy than fenofibrate (Ishibashi et al, 2018). We show here that pemafibrate significantly improved hippocampal LTP in male but not in female Tg mice, confirming the involvement of PPARα in synaptic plasticity in a sex specific manner.

While hippocampal LTP was improved by both pemafibrate and bexarotene treatments of male Tg mice, pemafibrate administration increased expression of both GluN2A and GluA1 whereas bexarotene only increased expression of GluA1. Although PPAR/RXR heterodimers are permissive (Evans & Mangelsdorf, 2014), it was previously demonstrated that the conformation of the ligand-receptor complexes and the nature of their interaction with co-regulators can differently modulate the transcription of target genes (Dowell et al, 1997; Perez et al, 2012; Schulman et al, 1998). We therefore hypothesize that due to their different affinities for different cofactors, bexarotene could upregulate only GluA1 whereas pemafibrate is able to drive the expression of both GluA1 and GluN2A subunits. Consequently, LTP improvement observed upon RXR and PPARα activation relies mainly on GluA1, but we cannot exclude that GluN2A could also be involved when PPARα is activated by pemafibrate. Although this study strongly supports that targeting PPARα could be an effective strategy to improve synaptic plasticity deficits related to cognitive defects (D'Orio et al, 2018), it presents some limitations. Our study was limited to the 5xFAD mouse model of AD. Therefore, further investigations are needed to confirm whether PPARα could be an interesting target in other mouse models of neurodegenerative diseases including Alzheimer, Parkinson and Huntington diseases, as well as multiple and amyotrophic lateral sclerosis, in which cognitive impairments occur. These mouse models do not fully recapitulate all pathological changes observed in patients and translating synaptic plasticity changes in mice with cognitive deficits in humans is challenging. However, based on the observations that bexarotene improves cognition in mouse models, we previously

reported that Targretin® (bexarotene) improved cognition in a patient with mild AD (Pierrot et al, 2016). In the same way, pemafibrate is utilized in human phase III clinical trials (Araki et al, 2018; Ishibashi et al, 2018) and investigating its effects on cognition in humans could be an interesting translational study based on our results.

Despite these limitations, we report here a sex regulated gene dosage effect of PPARα on synaptic plasticity. In animal models, sex differences should be considered rather than making the choice of the best responder. In humans, sex differences exist in the vulnerability, incidence, manifestation and treatment of numerous neurological and psychiatric diseases (Riecher-Rossler, 2017). Our results outline the importance to decipher sex differences in neurodegenerative diseases, including AD (Ferretti et al, 2018) with complex cognitive and neuropsychiatric symptoms, in order to define new sex-specific therapeutic strategies.

Materials and Methods

Animals

All animal procedures used in the study were carried out in accordance with institutional and European guidelines as certified by the local Animal Ethics Committee. Both pregnant Wistar rats used for embryonic cell cultures of either sex were obtained from Université catholique de Louvain (UCL, Brussels, Belgium) animal facilities. All protocols were approved by the local ethical committee of the UCL. 5xFAD (Oakley et al, 2006) mice were obtained from Jackson Laboratories (strain: B6SJL-Tg (APPSwFlLon, PSEN1*M146L*L286V) 6799Vas/Mmjax), bred as heterozygous 5xFAD mice. 5-6 months old PPARα deficient (*Ppara*$^{-/-}$) mice were used (Lee et al, 1995). Age-matched non-transgenic wild type littermates were used as controls. Experiments done with male and female separately were indicated. Animals were housed on a 12 hours light/dark cycle in standard animal care facilities.

Reagents and antibodies

When unmentioned, reagents for cell culture, western blotting and calcium imaging were purchased from Thermo Fisher Scientific (Waltham, MA, USA). Antibodies were purchased as indicated: Primary antibodies: mouse monoclonal anti-Glutamate Receptor 2 (6C4), rabbit monoclonal anti-GluA1 (C3T) and anti-GluN2A antibodies (Merck Millipore, Burlington, MA, USA, catalog nos. MAB397, 04-855 and 07-632, respectively); mouse monoclonal anti-GluN2B (BD Biosciences, San Jose, CA, USA, catalog no. 610417); goat polyclonal anti-SYNGAP (Bio-Connect life sciences, Huissen, The Netherlands, catalog no. LS-C154908) and mouse monoclonal anti-ABCA1 (Abcam, Cambridge, UK, cat no. ab18180, respectively); mouse

monoclonal anti-α tubulin and mouse monoclonal anti-MAP2 (Sigma-Aldrich, St-Louis, MO, USA, catalog nos. T6074 M4403 and A2066, respectively); anti-Transferrin Receptor mouse monoclonal antibody (H68.4) (Thermo Fisher Scientific, Waltham, MA, USA, catalog no. 13-6800). Secondary antibodies: donkey anti-rabbit and -mouse IgG horseradish (HRP) linked (GE Healthcare-Life Sciences, Little Chalfont, UK, catalog nos. NA934 and NA931, respectively); Alexa Fluor 647 goat anti-mouse IgG1, 488 chicken anti-goat IgG (H+L) and 568 goat anti-rabbit IgG (H+L) (Thermo Fisher Scientific, Waltham, MA, USA, catalog nos. A21240, A21467 and A11036, respectively).

Cell cultures

Hippocampal and cortical neuronal cultures were prepared from embryonic day 17 (E17) to E18 Wistar rats or P0-P1 pups from *Ppara*$^{-/-}$ and wild-type (*Wt*) mice from the same genetic background of either sex. Pregnant rats and mice were euthanized with CO_2. Hippocampi and cortices were isolated as previously described (Pierrot et al, 2013; Seibenhener & Wooten, 2012) with slight modifications. Briefly, hippocampal neurons were dissociated by incubation (15 min, 37°C) in 0.25% Trypsin-EDTA and triturated in Hank's Balanced Salt Solution without $CaCl_2$ and $MgCl_2$ supplemented with 10mM HEPES. Hippocampal and cortical cells were plated in culture dishes (1.5 and 4×10^5 cells/cm^2, respectively) pre-treated with 10 µg/ml poly-L-lysine (Sigma, St. Louis, MO, USA) in phosphate buffered saline (PBS) and cultured for 13-14 days *in vitro* in Neurobasal medium supplemented with 2% (v/v) B-27 medium and 0.5 mM L-glutamine without antibiotic solution prior to analyses. Hippocampal cells were pre-plated in a neuronal plating medium (Minimal Essential Medium (MEM) with Earl's salt supplemented with 2 mM glutamine, 330 µM D-Glucose (Sigma-Aldrich, St-Louis, MO, USA,

catalog no. G7528) and 5% fetal bovine serum (Biowest, Nuaillé,France, catalog no. S1820)) during 4-5h prior to Neurobasal medium described above. The cultures were maintained at 37°C under a 5% CO_2 atmosphere and half of the medium was renewed every 2-3 days.

Recombinant viruses and infection

Ppara and scramble shRNA containing Adeno-Associated Virus (AAV) were purchased from Vectors Biolabs (Malvern, PA, USA, catalog nos. shADV-269120 and 7045, respectively). For Ppara silencing, an AAV9-ShPpara (3.9×10^{13} GC/mL), containing a shRNA sequence (CCCTTATCTGAAGAATTCTTA) targeting both rat and mouse Ppara (Genbank RefSeq: NM_013196) and enhanced green fluorescent protein (eGFP) reporter gene, was produced. The expressions of Ppara and eGFP were driven by a U6 and a CMV promoter, respectively. An AAV9-GFP-U6-scramble-shRNA (AAV-ShSc, 4.7×10^{13} GC/mL) was used as a control. Cultures were transduced on 4th day *in vitro* (4 DIV) using AAV-ShPpara or AAV-ShSc at a multiplicity of infection of 12000 overnight. Then, infection medium was replaced by fresh culture medium every two days up to analysis (between 13-14 DIV).

Treatments and oral gavage

Treatments: cultured cells and hippocampal organotypic tissue cultures were treated for 24h with 100 nM and 300 nM bexarotene in 0.0002% DMSO (Targretin®), respectively. Control cells were treated with 0.0002% DMSO. For cell calcium imaging, neurons were challenged with 50 µM NMDA (Sigma-Aldrich, St-Louis, MO, USA, catalog no. M3262) or 50 µM AMPA (Tocris, Bristol, UK, catalog no. 1074) in the presence of 1 µM tetrodotoxin, a selective inhibitor of Na^+ channel conductance used to block spontaneous $[Ca^{2+}]_i$ transients in neurons (Tocris, Bristol,

UK, catalog no. 1078). For LTP measurements done on acute hippocampal slices from transgenic 5xFAD mice (9-10 mo) injected with AAV-Sh constructs, slices were treated with 4 µM bexarotene in aCSF (see below) for 2h30min prior to high frequency stimulation (see below).

Oral gavage: age-matched non-transgenic wild type and 5xFAD mice (9-10 mo) were treated for 12 days by oral gavage with 100 mg/kg/day b.wt. bexarotene or vehicle (water) or with 1 mg/kg/day b.wt. pemafibrate (at 12 mo) (Hennuyer et al, 2016) (MedChemExpress, Monmouth Junction, NJ, USA, catalog no. HY-17618) or vehicle (water 0.1% Tween 80).

Biotinylation and purification of plasma membrane-associated proteins.

13-14 DIV cultured cells seeded at 4.10^5 cells/cm^2 were washed with Krebs-HEPES buffer (see below). Cells were incubated with 1.6 mL of EZ-Link™ Sulfo-NHS-Biotin (Thermo Fisher Scientific catalog no. 21217) at 1.5 mg/mL in PBS for 30 min at 4 °C with mild shaking. Cells were then washed twice with cold PBS containing 100 mM glycine and incubated with the same solution for 45 min at 4 °C to quench the unbound biotin reagent. Cells were solubilized in lysis buffer containing 25 mM Tris-HCl pH 6.8, 0.5% (v/v) Triton X-100, 0.5% (v/v) Nonidet P-40 supplemented with proteases inhibitors for 1 h at 4°C with vigorous shaking. After centrifugation at 16 000 g at 4°C for 20 min, 300 µL of supernatant were incubated with an equal volume of Pierce™ Streptavidin Agarose beads suspension (Thermo Fisher Scientific catalog no. 20349) for 1 h at room temperature. After centrifugation (16 000 g, 15 min, 4°C), supernatants were collected for analysis of the non-biotinylated intracellular fraction. Biotinylated cell surface proteins contained in the pellet were washed two times with 600 µL lysis buffer and two times in

Krebs-HEPES buffer. The samples were eluted in 50 µL loading buffer (see below), boiled at 95 °C for 5 min.

Western blotting

Cells in culture were washed, scraped off in PBS and centrifuged for 2 min at 16 000 g. Pellets were sonicated in lysis buffer (125 mM Tris (pH 6.8), 20% glycerol, and 4% sodium dodecyl sulfate) with cOmplete Protease Inhibitor Cocktail (Roche, Bâle, Switzerland, catalog no. 11697498001). For brain proteins extraction, samples were homogenized in RIPA buffer (1% NP40, 0.5% deoxycholic acid, 0.1% SDS, 150 mM NaCl, 1 mM EDTA, 50 mM Tris, pH 7.4) containing proteases and phosphatases inhibitors cocktail (Roche, Basel, Switzerland, catalog no. 04906837001). The samples were clarified by centrifugation at 20 000g and the protein concentration was determined using a Bicinchoninic Acid Assay (BCA) kit. Samples were heated for 10 min at 70°C in loading buffer (lysis buffer containing 10 % 2-mercaptoethanol and 0.004 % bromophenol blue).

Cell and brain lysates (40 µg and 60 µg of proteins, respectively) were analyzed by Western blotting using 4-12 % Nupage^{TM} bis-Tris gels. Nitrocellulose membranes were incubated overnight at 4 °C with the following primary antibodies: anti-Glutamate Receptor 2 (GluA2, 1:1000); anti-GluA1 (1:500); anti-GluN2A (1:250); anti-GluN2B (1:500); anti-ABCA1 (1:1000); anti-α tubulin (1:4000) and anti-Transf R (1:1000). Blots were incubated with HRP peroxidase-conjugated secondary antibodies (1:10000), revealed by ECL (Amersham Pharmacia, Buckinghamshire, UK, catalog nos. ORT2655-2755), and quantified using the Quantity One^{TM} software (Bio-Rad Laboratories, Hercules, CA, USA). α-tubulin or Transf R were used as internal standards to normalize protein load in gels.

RNA extraction and real time PCR

Total RNA was isolated by TriPure Isolation Reagent (Roche, Basel, Switzerland, catalog no. 11667165001) according to the manufacturer's protocol. RNA samples were resuspended in DEPC-treated water. Reverse transcription was carried out with the iScript cDNA synthesis Kit (Bio-Rad Laboratories, Hercules, CA, USA, catalog no. 1708891) using 1 µg of total RNA in a total volume reaction of 20 µL. Real-time PCR was performed for the amplification of cDNAs with specific primers (Sigma-Aldrich (St-Louis, MO), see Table S1).

Real-time PCR was carried out in a total volume of 25 µL containing 8 ng cDNA template, 0.3 µM of the appropriate primers and the IQ™ SYBR® Green Supermix 1x (Bio-Rad Laboratories, Hercules, CA, USA, catalog no. 1708885). The PCR protocol consisted of 40 amplification cycles (95°C for 30 s, 60°C for 45 s and 79°C for 15 s) and was performed using an iCycler IQ™ multicolor Real-Time PCR detection system (Bio-Rad Laboratories, Hercules, CA, USA), used to determine the threshold cycle (Ct). Melting curves were performed to detect nonspecific amplification products. A standard curve was established for each target gene using four-fold serial dilutions (from 100 to 0.097 ng) of a cDNA template mix prepared in the same conditions. The differences between the Ct of one condition and the control were measured and each sample was normalized with the relative expression levels of *Gapdh*.

Cytosolic free Ca^{2+} measurement in single neurons

For cytosolic free Ca^{2+} measurement, all recordings were carried out at 37°C in Krebs-HEPES buffer (10 mM HEPES, 135 mM NaCl, 6 mM KCl, 2 mM $CaCl_2$, 1.2 mM $MgCl_2$, 10 mM glucose, pH 7.4), as previously described (Doshina et al, 2017). Briefly, 50 µM NMDA or

AMPA were perfused with Krebs-HEPES buffer in the incubation chamber. Neurons were plated at a density of 1.8 10^5 cells/cm^2 on 15 mm round glass coverslips pre-coated with 10 µg/ml poly-L-lysine in PBS. 13-14 DIV cultured cells were incubated in the dark in presence of the Ca^{2+} indicator fura-2 acetoxymethylester (Fura-2 AM; catalog no. F1225) at a final concentration of 2 µM in Krebs-HEPES buffer for 30 min at room temperature. Coverslips were then washed and mounted in a heated (37°C) microscope chamber (1 ml). Cells were alternately excited (1 or 2 Hz) at 340 and 380 nm for 100 ms using a Lambda DG-4 Ultra High Speed Wavelength Switcher (Sutter Instrument, Novato, CA) coupled to a Zeiss Axiovert 200 M inverted microscope (X20 fluorescence objective) (Zeiss Belgium, Zaventem, BE). Images were acquired using a Zeiss Axiocam camera coupled to a 510 nm emission filter and analyzed with the Axiovision software. A total of 70-80 neurons was studied in each experiment and non-neuronal cells were excluded from the analysis as previously described by Pickering and coworkers (Pickering et al, 2008). Changes in intracellular calcium fluorescence were estimated from fluorescence emission intensity ratio F340/F380 (ΔF) obtained after excitation of cells at to wavelengths of 340nm and 380nm. These changes were expressed as normalized fluorescence where every measurement of ΔF was divided by the basal fluorescence (F0) value corresponding to the mean of signals measured during a period of 20 s in basal condition (prior to NMDA or AMPA). NMDA and AMPA responses were defined as a change of ΔF greater than 10 % relative to F0.

Stereotaxic injections

For stereotaxic surgery, 9-10 months old 5xFAD mice were anesthetized by intraperitoneal injection (i.p.) with a mixture of 160 mg/kg b.wt. Ketamine (Nimatek, Eurovet Animal Health

BV, Bladel, Netherlands) and 20 mg/kg b.wt. Xylazine (ROMPUN®, Bayer, Leverkusen, Germany). Ipsi and contra-lateral stereotaxic injections (left and right hemisphere, respectively) were performed at two sites in the hippocampal CA1 region (A/P, -1.8; L, +/-1.1; D/V, -1.3 and A/P, -2.5; L, +/-2.0; D/V, -1.5) millimeter relative to bregma (Paxinos G, Franklin KBJ. The mouse brain in stereotaxic coordinates. San Diego: Academic; 2001). Ipsilateral AAV-ShPpara (3.9×10^{13} GC/mL) or contralateral AAV-ShSc (4.7×10^{13} GC/mL) stereotaxic injection (5 µL in total of each; 2.5 µL per site of injections) were performed using a 10 µL Hamilton syringe (Filter Service, Eupen, Belgium, catalog no. HA 7635-01) at a speed of 1 µL per min. After injection, the needle was kept in place for additional 3 min before gentle withdrawal. All analyses were performed 3 weeks post-injection.

Electrophysiology-Long term potentiation (LTP)

Males and females PPARα deficient (*Ppara*$^{-/-}$) and transgenic (Tg) 5xFAD mice at 5-6 and 9-10 months of age, respectively, were anesthetized with pentobarbital (Nembutal, i.p. 100 mg/kg b.wt.) and decapitated. Age-matched wild-type (Wt) of the same genetic background were used as controls. The hippocampus was dissected and cut in 450 µm-thick slices with a tissue chopper. The slices were transferred into the recording chamber and kept in interface at 28°C for 1.5 h. Hippocampal slices were perfused with artificial cerebrospinal fluid (aCSF) with the following composition: 124 mM NaCl, 5 mM KCl, 26 mM $NaHCO_3$, 1.24 mM NaH_2PO_4, 2.5 mM $CaCl_2$, 1.3 mM $MgSO_4$, 10 mM glucose, bubbled with a mixture of 95 % O_2 and 5 % CO_2. The perfusion rate of aCSF was 1 ml/min. LTP was induced by applying one train (100 Hz, 1s). A bipolar twisted nickel-chrome electrode (50 µm each) was used to stimulate Schaffer's collaterals. Extracellular field excitatory postsynaptic potentials (fEPSP) were recorded in the

stratum radiatum of the CA1 region with low resistance (2-5 MΩ) glass microelectrodes filled with aCSF (Villers & Ris, 2013). Test stimuli were biphasic (0.08 ms for each pulse) constant-voltage pulses delivered every minute with an intensity adjusted to evoke an approximate 40 % maximal response. The slope of the fEPSP was measured on the average of four consecutive responses. Stimulation, data acquisition and analysis were performed using the WinLTP program (Anderson & Collingridge, 2007) (Website: www.winltp.com). For each slice, the fEPSP slopes were normalized with respect to the mean slope of the fEPSPs recorded during the 30 min period preceding induction of LTP.

Confocal microscopy and image processing and analysis

Cells were seeded at 10^5 cells/cm^2 on 15 mm round glass coverslips pre-coated with 10 µg/ml poly-L-lysine in PBS, fixed 15 min with 4% v/v formaldehyde at room temperature then washed in PBS and permeabilized 1 h with 0,4% Triton X100 (v/v) in PBS containing 3% bovine serum albumin (Sigma-Aldrich, St-Louis, MO, USA, catalog no. A7906). After three washes in PBS, cells were incubated 1h at room temperature with primary antibodies: anti-SynGAP (1:50), -MAP2 (1:1000), and -GluA1 (1:100). After three PBS washes, cells were incubated for 1h with 5 µg/ml Alexa-labelled secondary antibodies (1:200). After three additional PBS washes, preparations were mounted in EverBrite™ (VWR, Oud-Heverlee, Belgium, catalog no. 23003) and were examined with a LSM 510 META confocal microscope (Zeiss, Jena, Germany) using a Plan-Apochromat 63X/1.4 oil DIC objective. The non-overlapping between GluA1 and SynGAP was determined on line intensity profiles. After threshold value determination to define the effective dynamic range, peaks were identified and classified into three categories: (i) only red, indicating non-overlapping of GluA1 with SynGAP; (ii) only green, indicating non-overlapping

of SynGAP with GluA1; and (iii) red+green, indicating overlapping between GluA1 and SynGAP. The abundance of peaks in each category was then expressed as percentage of total peaks. Cluster size of GluA1 puncta were quantified using AxioVision 4.8.2. Images were first resampled to isolate the red channel for analysis (resampling step) and then segmented to isolate only the grey values between 80 and 255 (segmentation step). Images were then binarized, with the white areas corresponding to the GluA1 clusters (binary scrap step), and small holes in these clusters were filled up (binary fill step). After visual comparison of these white areas with the clusters on the initial pictures, the average area of clusters was measured with the AxioVision software in the "automatic measurement" mode and data were exported in Excel for calculation and statistical analysis.

Statistics

Statistical analyses were performed using GraphPad Prism 7.01 (GraphPad Software, La Jolla, CA, USA). The Shapiro-Wilk test was used to test for the normality of data. Parametric testing procedures (Student's *t*-test or one-way analysis of variance (ANOVA) followed by Bonferroni's multiple-comparison post-test when many subgroups were compared) were applied for normally distributed data, otherwise nonparametric tests were used (Mann-Whitney or Kruskal-Wallis tests followed by Dunn's multiple-comparison post-test when many subgroups were compared). Total number of samples (n) analyzed in all experimental conditions (number of repeated measurements) is indicated in figures legends. Results were presented as mean ± SEM and statistical significance was set at P values < 0.05 (two-tailed tests, excepted for Morris water maze experiments only a one-sided P values is presented) ($*P<0.05$, $**P<0.01$; $***P<0.001$). For LTP, statistical differences of the means (± SEM) were measured on the last 30 min before

the end of the recording. Graphical data are represented as plot data with individual points overlaid.

Acknowledgments: We thank the Fondation Louvain for a support to N.P., the Netherlands Brain Bank for providing us with human brain samples, F. Saez-Orellana, PhD (IoNS, Brussels, Belgium) for discussion and Pr. L. Hue for his critical evaluation of the results and editing the manuscript. This work was supported by the Belgian Fonds pour la Recherche Scientifique, Interuniversity Attraction Poles Program-Belgian State-Belgian Science Policy, The Belgian Fonds de la Recherche Scientifique Médicale, the Queen Elisabeth Medical Foundation and the Fondation pour la Recherche sur la Maladie d'Alzheimer.

Author contributions: NP and JNO designed research. NP, AD and FR performed primary cultures, infection, biochemical experiments and calcium imaging. NP performed pemafibrate gavage, immunocytochemistry and analyzed data. LR performed electrophysiological analyses. ICS and ID performed bexarotene and pemafibrate gavages, stereotaxic injections, ORT/MWM behavioral experiments and immunohistochemistry. O.S. performed MWM behavioral experiments. DT performed confocal microscopy/images analyzes. PG provided his expertise in calcium imaging. LM did cultures of hippocampal slices. IW, ICS, JPB and KL provided 5xFAD mice. BS, EB and FL provided *Ppara*$^{-/-}$ mice. NP and JNO wrote the manuscript.

Conflict of interest: We declare to have no competing financial interests.

Supplementary figures, Supplementary information, Table S1 and Source Data accompany this paper.

References

Anderson WW, Collingridge GL (2007) Capabilities of the WinLTP data acquisition program extending beyond basic LTP experimental functions. J Neurosci Methods 162**:** 346-356

Araki E, Yamashita S, Arai H, Yokote K, Satoh J, Inoguchi T, Nakamura J, Maegawa H, Yoshioka N, Tanizawa Y et al (2018) Effects of Pemafibrate, a Novel Selective PPARalpha Modulator, on Lipid and Glucose Metabolism in Patients With Type 2 Diabetes and Hypertriglyceridemia: A Randomized, Double-Blind, Placebo-Controlled, Phase 3 Trial. Diabetes Care 41**:** 538-546

Arevalo MA, Azcoitia I, Gonzalez-Burgos I, Garcia-Segura LM (2015) Signaling mechanisms mediating the regulation of synaptic plasticity and memory by estradiol. Horm Behav 74**:** 19-27

Barrier L, Ingrand S, Fauconneau B, Page G (2010) Gender-dependent accumulation of ceramides in the cerebral cortex of the APP(SL)/PS1Ki mouse model of Alzheimer's disease. Neurobiol Aging 31**:** 1843-1853

Bensinger SJ, Tontonoz P (2008) Integration of metabolism and inflammation by lipid-activated nuclear receptors. Nature 454**:** 470-477

Bliss TV, Collingridge GL (1993) A synaptic model of memory: long-term potentiation in the hippocampus. Nature 361**:** 31-39

Bookout AL, Jeong Y, Downes M, Yu RT, Evans RM, Mangelsdorf DJ (2006) Anatomical profiling of nuclear receptor expression reveals a hierarchical transcriptional network. Cell 126**:** 789-799

Chen HJ, Rojas-Soto M, Oguni A, Kennedy MB (1998) A synaptic Ras-GTPase activating protein (p135 SynGAP) inhibited by CaM kinase II. Neuron 20**:** 895-904

Chung KW, Lee EK, Lee MK, Oh GT, Yu BP, Chung HY (2018) Impairment of PPARalpha and the Fatty Acid Oxidation Pathway Aggravates Renal Fibrosis during Aging. J Am Soc Nephrol 29**:** 1223-1237

Corbett GT, Gonzalez FJ, Pahan K (2015) Activation of peroxisome proliferator-activated receptor alpha stimulates ADAM10-mediated proteolysis of APP. Proc Natl Acad Sci U S A 112**:** 8445-8450

D'Agostino G, Cristiano C, Lyons DJ, Citraro R, Russo E, Avagliano C, Russo R, Raso GM, Meli R, De SG et al (2015) Peroxisome proliferator-activated receptor alpha plays a crucial role in behavioral repetition and cognitive flexibility in mice. Mol Metab 4**:** 528-536

D'Orio B, Fracassi A, Ceru MP, Moreno S (2018) Targeting PPARalpha in Alzheimer's Disease. Curr Alzheimer Res 15**:** 345-354

Derkach VA, Oh MC, Guire ES, Soderling TR (2007) Regulatory mechanisms of AMPA receptors in synaptic plasticity. Nat Rev Neurosci 8**:** 101-113

Doshina A, Gourgue F, Onizuka M, Opsomer R, Wang P, Ando K, Tasiaux B, Dewachter I, Kienlen-Campard P, Brion JP et al (2017) Cortical cells reveal APP as a new player in the regulation of GABAergic neurotransmission. Sci Rep 7**:** 370

Dotson AL, Wang J, Chen Y, Manning D, Nguyen H, Saugstad JA, Offner H (2016) Sex differences and the role of PPAR alpha in experimental stroke. Metab Brain Dis 31**:** 539-547

Dowell P, Ishmael JE, Avram D, Peterson VJ, Nevrivy DJ, Leid M (1997) p300 functions as a coactivator for the peroxisome proliferator-activated receptor alpha. J Biol Chem 272**:** 33435-33443

Evans RM, Mangelsdorf DJ (2014) Nuclear Receptors, RXR, and the Big Bang. Cell 157**:** 255-266

Ferretti MT, Iulita MF, Cavedo E, Chiesa PA, Schumacher DA, Santuccione CA, Baracchi F, Girouard H, Misoch S, Giacobini E et al (2018) Sex differences in Alzheimer disease - the gateway to precision medicine. Nat Rev Neurol 14**:** 457-469

Gross B, Pawlak M, Lefebvre P, Staels B (2017) PPARs in obesity-induced T2DM, dyslipidaemia and NAFLD. Nat Rev Endocrinol 13**:** 36-49

Hennuyer N, Duplan I, Paquet C, Vanhoutte J, Woitrain E, Touche V, Colin S, Vallez E, Lestavel S, Lefebvre P et al (2016) The novel selective PPARalpha modulator (SPPARMalpha) pemafibrate improves dyslipidemia, enhances reverse cholesterol transport and decreases inflammation and atherosclerosis. Atherosclerosis 249**:** 200-208

Ishibashi S, Arai H, Yokote K, Araki E, Suganami H, Yamashita S (2018) Efficacy and safety of pemafibrate (K-877), a selective peroxisome proliferator-activated receptor alpha modulator, in patients with dyslipidemia: Results from a 24-week, randomized, double blind, active-controlled, phase 3 trial. J Clin Lipidol 12**:** 173-184

Jalouli M, Carlsson L, Ameen C, Linden D, Ljungberg A, Michalik L, Eden S, Wahli W, Oscarsson J (2003) Sex difference in hepatic peroxisome proliferator-activated receptor alpha expression: influence of pituitary and gonadal hormones. Endocrinology 144**:** 101-109

Lalloyer F, Wouters K, Baron M, Caron S, Vallez E, Vanhoutte J, Bauge E, Shiri-Sverdlov R, Hofker M, Staels B et al (2011) Peroxisome proliferator-activated receptor-alpha gene level differently affects lipid metabolism and inflammation in apolipoprotein E2 knock-in mice. Arterioscler Thromb Vasc Biol 31**:** 1573-1579

Lee SS, Pineau T, Drago J, Lee EJ, Owens JW, Kroetz DL, Fernandez-Salguero PM, Westphal H, Gonzalez FJ (1995) Targeted disruption of the alpha isoform of the peroxisome proliferator-activated receptor gene in mice results in abolishment of the pleiotropic effects of peroxisome proliferators. Mol Cell Biol 15**:** 3012-3022

Lefebvre P, Benomar Y, Staels B (2010) Retinoid X receptors: common heterodimerization partners with distinct functions. Trends Endocrinol Metab 21**:** 676-683

Mariani MM, Malm T, Lamb R, Jay TR, Neilson L, Casali B, Medarametla L, Landreth GE (2017) Neuronally-directed effects of RXR activation in a mouse model of Alzheimer's disease. Sci Rep 7**:** 42270

Middei S, Houeland G, Cavallucci V, Ammassari-Teule M, D'Amelio M, Marie H (2013) CREB is necessary for synaptic maintenance and learning-induced changes of the AMPA receptor GluA1 subunit. Hippocampus 23**:** 488-499

Montagne A, Zhao Z, Zlokovic BV (2017) Alzheimer's disease: A matter of blood-brain barrier dysfunction? J Exp Med 214**:** 3151-3169

Mounier A, Georgiev D, Nam KN, Fitz NF, Castranio EL, Wolfe CM, Cronican AA, Schug J, Lefterov I, Koldamova R (2015) Bexarotene-Activated Retinoid X Receptors Regulate Neuronal Differentiation and Dendritic Complexity. J Neurosci 35**:** 11862-11876

Moutinho M, Landreth GE (2017) Therapeutic potential of nuclear receptor agonists in Alzheimer's disease. J Lipid Res 58**:** 1937-1949

Nam KN, Mounier A, Fitz NF, Wolfe C, Schug J, Lefterov I, Koldamova R (2016) RXR controlled regulatory networks identified in mouse brain counteract deleterious effects of Abeta oligomers. Sci Rep 6**:** 24048

Oakley H, Cole SL, Logan S, Maus E, Shao P, Craft J, Guillozet-Bongaarts A, Ohno M, Disterhoft J, Van EL et al (2006) Intraneuronal beta-amyloid aggregates, neurodegeneration, and neuron loss in transgenic mice with five familial Alzheimer's disease mutations: potential factors in amyloid plaque formation. J Neurosci 26**:** 10129-10140

Perez E, Bourguet W, Gronemeyer H, de Lera AR (2012) Modulation of RXR function through ligand design. Biochim Biophys Acta 1821**:** 57-69

Pickering M, Pickering BW, Murphy KJ, O'Connor JJ (2008) Discrimination of cell types in mixed cortical culture using calcium imaging: a comparison to immunocytochemical labeling. J Neurosci Methods 173**:** 27-33

Pierrot N, Lhommel R, Quenon L, Hanseeuw B, Dricot L, Sindic C, Maloteaux JM, Octavea JN, Ivanoiu A (2016) Targretin Improves Cognitive and Biological Markers in a Patient with Alzheimer's Disease. J Alzheimers Dis 49**:** 271-276

Pierrot N, Tyteca D, D'auria L, Dewachter I, Gailly P, Hendrickx A, Tasiaux B, Haylani LE, Muls N, N'kuli F et al (2013) Amyloid precursor protein controls cholesterol turnover needed for neuronal activity. EMBO Mol Med 5**:** 608-625

Raza-Iqbal S, Tanaka T, Anai M, Inagaki T, Matsumura Y, Ikeda K, Taguchi A, Gonzalez FJ, Sakai J, Kodama T (2015) Transcriptome Analysis of K-877 (a Novel Selective PPARalpha Modulator (SPPARMalpha))-Regulated Genes in Primary Human Hepatocytes and the Mouse Liver. J Atheroscler Thromb 22**:** 754-772

Riecher-Rossler A (2017) Sex and gender differences in mental disorders. Lancet Psychiatry 4**:** 8-9

Roy A, Jana M, Corbett GT, Ramaswamy S, Kordower JH, Gonzalez FJ, Pahan K (2013) Regulation of cyclic AMP response element binding and hippocampal plasticity-related genes by peroxisome proliferator-activated receptor alpha. Cell Rep 4**:** 724-737

Schmitt WB, Sprengel R, Mack V, Draft RW, Seeburg PH, Deacon RM, Rawlins JN, Bannerman DM (2005) Restoration of spatial working memory by genetic rescue of GluR-A-deficient mice. Nat Neurosci 8**:** 270-272

Schulman IG, Shao G, Heyman RA (1998) Transactivation by retinoid X receptor-peroxisome proliferator-activated receptor gamma (PPARgamma) heterodimers: intermolecular synergy requires only the PPARgamma hormone-dependent activation function. Mol Cell Biol 18**:** 3483-3494

Seibenhener ML, Wooten MW (2012) Isolation and culture of hippocampal neurons from prenatal mice. J Vis Exp

Staels B, Dallongeville J, Auwerx J, Schoonjans K, Leitersdorf E, Fruchart JC (1998) Mechanism of action of fibrates on lipid and lipoprotein metabolism. Circulation 98**:** 2088-2093

Tata JR (1994) Autoregulation and crossregulation of nuclear receptor genes. Trends Endocrinol Metab 5**:** 283-290

Venkateswaran A, Laffitte BA, Joseph SB, Mak PA, Wilpitz DC, Edwards PA, Tontonoz P (2000) Control of cellular cholesterol efflux by the nuclear oxysterol receptor LXR alpha. Proc Natl Acad Sci U S A 97**:** 12097-12102

Villers A, Ris L (2013) Improved preparation and preservation of hippocampal mouse slices for a very stable and reproducible recording of long-term potentiation. J Vis Exp

Warden A, Truitt J, Merriman M, Ponomareva O, Jameson K, Ferguson LB, Mayfield RD, Harris RA (2016) Localization of PPAR isotypes in the adult mouse and human brain. Sci Rep 6**:** 27618

Watt MJ, Southgate RJ, Holmes AG, Febbraio MA (2004) Suppression of plasma free fatty acids upregulates peroxisome proliferator-activated receptor (PPAR) alpha and delta and PPAR coactivator 1alpha in human skeletal muscle, but not lipid regulatory genes. J Mol Endocrinol 33**:** 533-544

Yamazaki Y, Abe K, Toma T, Nishikawa M, Ozawa H, Okuda A, Araki T, Oda S, Inoue K, Shibuya K et al (2007) Design and synthesis of highly potent and selective human peroxisome proliferator-activated receptor alpha agonists. Bioorg Med Chem Lett 17**:** 4689-4693

Zolezzi JM, Santos MJ, Bastias-Candia S, Pinto C, Godoy JA, Inestrosa NC (2017) PPARs in the central nervous system: roles in neurodegeneration and neuroinflammation. Biol Rev Camb Philos Soc 92**:** 2046-2069

Figure Legends

Figure 1. RXR activation ameliorates LTP, AMPA-induced responses and GluA1 expression.

(A, **B)** Transgenic (Tg) 5xFAD and wild type (Wt) mice treated at 9-10 months old with bexarotene (bex) (100mg/kg/day) or vehicle (veh) by gavage (12 days). (**A**) CA1 LTP in hippocampal slices of Tg+veh (n=8) and Tg+bex (n=7) compared to Wt+veh (n=6). ∗∗∗P<0.001, Student's t test. (**B**) Representative Western blot of hippocampal lysates from Wt and Tg mice. Right panel: GluN2A, GluN2B and GluA1/α tubulin ratios. Results are expressed as percentage of Wt+veh (n=5 for each); compared to Wt+veh: ##P<0.01, ###P<0.001 compared to Tg+veh: ∗P<0.05, ANOVA followed by Bonferroni's multiple-comparison post-test). **(C)** Representative Western blot of control (Co) and 100 nM bex treated (24h) cell lysates from cortical cultures. Right panel: GluN2A, 2B and GluA1/α tubulin ratios. Results are expressed as percentage of respective Co (Co n=18 and bex n=17 of each analyzed in 10 independent experiments, ∗∗∗P<0.001, Mann-Whitney test). **(D)** Normalized fluorescence intensity of Fura-2 AM in Co and bex treated cortical cells in presence of AMPA (right panel) and NMDA (left panel). Insets: amplitude of AMPA (Co n=257, bex n=148 cells analyzed in 6 and 5 independent experiments) and NMDA responses (Co n=307, bex n=177 in 7 and 6 independent experiments); ∗∗∗P<0.001, ns: not significant (P>0.05), Mann-Whitney test). **(E)** Cell surface biotinylation analyzed by Western blot (left panel). Right panel: GluA1/Transferrin Receptor (Transf R) ratios. Results are expressed as percentage of respective Co (n=6 of each in 3 independent experiments, ∗P<0.05, ∗∗∗P<0.001, Student's t-test). **(F)** Co and bex treated MAP2 positive neurons immunolabeled for GluA1 (red) and SynGAP (green). Scale bar: 5 µm. **(G**, **H)** Representative profiles of the regions

highlighted by the rectangles in merge pictures in (**F**). In (**H**), the number of GluA1 (red numbers), SynGAP (green numbers) and GluA1/SynGAP overlapping (black numbers) peaks were quantified on >60 profiles per condition from 4 independent experiments. Results are expressed as percentage of total peaks from all the profiles. **(I)** Quantification of synaptic GluA1 puncta-cluster size (in μm^2) in Co or bex treated neurons. Results of >900 (from 23 images) and 1700 clusters (from 33 images) for Co and bex treated neurons, respectively. ∗∗∗P<0.001, Student's t-test.

Data information: data are presented as mean ± SEM.

Figure 2. Absence of PPARα abrogates GluA1 expression and AMPA responses induced by RXR activation.

(A) RT-qPCR analyses of *Ppara*, *Pparb*, *Pparg*, *Rxra*, *Rxrg* and *Nr1h2* mRNA levels in control (Co) and bexarotene (bex, 100 nM/24h) treated cortical cultures (n=6-10 in 3-5 independent experiments), ∗∗∗P<0.001, Student's *t*-test. **(B)** RT-qPCR analyses of *Gria1* and *Abca1* mRNA levels in 3 independent experiments from cortical cells prepared from wild type (*Wt*, n=6 of each) and *Ppara* deficient *(Ppara*$^{-/-}$, n=10 of each*)* mice treated or not with bex. Results are expressed as percentage of corresponding non-treated cells (compared to *Wt*: ∗P<0.05, ∗∗P<0.01; compared to *Ppara*$^{-/-}$: ###P<0.001 (Student's *t*-test)). **(C**, **D)** Representative Western blots of cortical cell lysates from *Wt* (**C**) and *Ppara*$^{-/-}$ (**D**) cultures treated or not with bex. Right panels: GluA1 and ABCA1/α tubulin ratios. Results are expressed as percentage of respective untreated *Wt* or *Ppara*$^{-/-}$ (*Wt*: n=6; *Wt* + bex: n=7; *Ppara*$^{-/-}$: n=8; *Ppara*$^{-/-}$ + bex: n=7 of each analyzed in 3 independent experiments, ∗P< 0.05, ∗∗P< 0.01, Student's *t*-test, except for ABCA1 in *Wt* + bex: Mann-Whitney test). **(E**, **F)** AMPA-induced calcium fluorescence in *Wt*

(**E**) and *Ppara*$^{-/-}$ (**F**) cortical cells treated with bex. Insets: AMPA responses amplitude (*Wt* n=320, *Wt* + bex n=118 and *Ppara*$^{-/-}$ n=430, *Ppara*$^{-/-}$ + bex n=374 cells analyzed in 3-6 independent experiments; ∗∗∗*P*<0.001, ns: not significant (*P*>0.05), Mann-Whitney test).

Data information: data are presented as mean ± SEM.

Figure 3. PPARα deficiency impairs LTP and GluA1 expression in male mice.

(A) PPARα mRNA levels analyzed in the hippocampus from female (♀) and male (♂) wild type (*Wt*) mice by RT-qPCR and semi-quantitative RT-PCR (left and right panels, respectively). Results are expressed as percentage of corresponding ♀ (n=6 of each, ∗∗∗*P*<0.001, Student's *t* test). **(B**, **E)** CA1 LTP in hippocampal slices from 5-6 months old male (♂) and female (♀) wild type (*Wt*, in (**B**)) and *Ppara* deficient *(Ppara*$^{-/-}$, in (**E**)) mice (n=6 in each group). ∗∗∗*P*<0.001, Student's *t* test. **(C**, **F)** RT-qPCR analyses of *Grin2A* and *2B* and *Gria1* mRNA levels in the hippocampus from female (♀) and male (♂) *Wt* (n=11) and *Ppara*$^{-/-}$ (n=6-8) mice. Results are expressed as percentage of corresponding ♀ (in (**C**) compared to *Wt* ♀: ∗∗*P*<0.01, Mann-Whitney test; in (**F**) compared to *Ppara*$^{-/-}$ ♀: ∗∗*P*<0.01, Student's *t* test). **(D**, **G)** Representative Western blots of hippocampal lysates from female (♀) and male (♂) *Wt* and *Ppara*$^{-/-}$ mice. Right panels: quantification of GluN2A, GluN2B and GluA1/α tubulin ratios. Results are expressed as percentage of corresponding ♀ (in (**D**) compared to *Wt* ♀: ∗∗*P*<0.01, in (**G**) compared to *Ppara*$^{-/-}$ ♀: ∗∗∗*P*<0.001, Student's *t* test) (*Wt* n=8-10, *Ppara*$^{-/-}$ n=7 for each condition).

Data information: data are presented as mean ± SEM.

Figure 4. LTP improvement by RXR activation is PPARα and sex dependent.

(A) Schematic drawing of the top view of a mouse brain. Stars: ipsi and contralateral injection sites of *Ppara* and scramble shRNA AAV (AAV-ShPpara (orange) and -ShSc (blue)). Dashed line represents the plane of the coronal section used in (**B, C** and **D**) for biochemical analyses. **(B)** RT-qPCR analyses of *Ppara* mRNA levels in male (♂) and female (♀) Tg mice hippocampi AAV-ShSc and -ShPpara injected at 9-10 months old. Results are expressed as percentage of AAV-ShSc injected male mice (n=4 of each; ∗*P*<0.05, ∗∗*P*<0.01, ∗∗∗*P*<0.001, ns: not significant (P>0.05), ANOVA followed by Bonferroni's multiple-comparison post-test). Right panels: PPARα semi-quantitative RT-PCR. **(C**, **D)** Representative Western blots of hippocampal lysates from male (♂, in **C**) and female (♀, in **D**) Tg mice AAV-ShSc and -ShPpara injected. Right panels: quantification of GluN2A, GluN2B and GluA1/α tubulin ratios in male (in **C**) and female (in **D**) Tg mice AAV-ShSc and -ShPpara injected. Results are expressed as percentage of corresponding Tg mice AAV-ShSc injected (n=4 in each condition, ∗∗*P*<0.01, Student's *t* test; ns: not significant (P>0.05)). **(E**, **F)** CA1 LTP in hippocampal slices from male (♂, in (**E**)) and female (♀, in (**F**)) transgenic (Tg) 5xFAD mice (9-10 mo) AAV-ShPpara and -ShSc injected and perfused with 4 µM bexarotene (bex) (n=4 in each group, ∗∗∗*P*<0.001, Student's *t* test).

Data information: data are presented as mean ± SEM.

Figure 5. Sex specific improvement of LTP by pemafibrate.

(A, **B)** Male (♂) and female (♀) transgenic (Tg) 5xFAD mice treated at 12 months old with pemafibrate (pema) (1 mg/kg/day) or vehicle (veh) by gavage (12 days). CA1 LTP in hippocampal slices of male Tg + veh (n=6) and Tg + pema mice (n=8) in (**A**) and female Tg + veh (n=4) and Tg + pema mice (n=6) in (**B**), ∗∗∗*P*<0.001, Student's *t* test. **(C**, **E)** RT-qPCR analyses of *Grin2A* and *2B* and *Gria1* mRNA levels in the hippocampus from male Tg mice

treated with pema (n=8) or veh (n=6 for each condition) in (**C**) and from female Tg mice treated with pema (n=6) or veh (n=4 of each) in (**E**). Results are expressed as percentage of corresponding Tg + veh (∗*P*<0.05, ∗∗*P*<0.01; Student's *t*-test). **(D**, **F)** Representative Western blots of hippocampal lysates from male (**D**) and female (**F**) Tg mice treated or not with pema. Right panels: quantification of GluN2A, GluN2B and GluA1/α tubulin ratios. Results are expressed as percentage of corresponding Tg + veh (Tg + veh n=5 and Tg + pema n=6 of each, ∗*P*<0.05, Student's *t*-test).

Data information: data are presented as mean ± SEM.

Figure 6. Sex and PPARα specific effects on GluA1 expression and synaptic plasticity.

(A) Schematic representation of LXR/RXR and PPARα/RXR heterodimers bound to a specific DNA sequence. LXR/RXR drives the expression of ABCA1 and PPARα/RXR drives the expression of CREB, which in turn, drives the expression of GluA1. **(B)** PPARα and GluA1 expression are higher (>) in male (♂) than in female (♀) mice. The gene dosage effect of PPARα on GluA1 expression leads to a better (>) synaptic plasticity in male than in female mice.

Supplementary Figure Legends

Figure S1. RXR activation improves cognition in an AD mouse model, independently of brain amyloid plaque load.

(A) 9-10 months old wild-type (Wt) mice treated with bexarotene (bex) (100mg/kg/day) or vehicle (veh) by gavage (12 days). CA1 LTP in hippocampal slices of Wt male + bex (n=4) was compared to Wt + veh (n=4). P>0.05, Student's t test. **(B)** 9-10 months old 5xFAD transgenic

(Tg) and wild type (Wt) mice treated with bexarotene (bex) (100mg/kg/day) or vehicle (veh) by gavage. Cognition in Tg+veh (n=7) and Wt+veh (n=5) mice was measured in the object recognition task (ORT). Bex treatment increased OR memory in Tg mice (Tg+bex, n=8). Recognition memory is expressed as exploratory preference in retention test, 3h post-training (compared to Wt+veh: #P<0.05; compared to Tg+veh: ∗P<0.05, ANOVA followed by Bonferroni's multiple-comparison post-test). **(C)** Cognitive performance in Tg mice in Morris Water Maze (MWM) test was improved by 10 days treatment with bex (training started following 5 days of treatment). Latency to reach the escape platform decreased on the 5th day of training in Wt and Tg mice treated with bex (n=5 in each group; ∗P<0.05, ∗∗∗P<0.001 by ANOVA analysis followed by Bonferroni's multiple-comparison post-test, one-sided P-values are presented for MWM experiments only). **(D)** Swim speed and path length measured in MWM test in Tg treated with bex or veh for 10 days (n=5 in each group). **(E)** Amyloid plaque load measured on brain sections stained with anti-Aβ antibody in cortex, hippocampus, subiculum and hippocampal CA1 region. Results are expressed as percentage of Tg+veh (n=5 for each condition; P>0.05, Student's t-test).

Data information: data are presented as mean ± SEM.

Figure S2. RXR activation increases GluA1 expression in primary hippocampal neurons and organotypic hippocampal slices without modifying GluA2 expression.

(A, **B)** Representative Western blots of control (Co) and 100 nM bexarotene (bex) treated (24h) primary hippocampal neurons in cultures at 13-14 DIV (**A**) and 300 nM bex treated (24h) organotypic hippocampal slices at 7 DIV (**B**) lysates. Expression of GluA1 was monitored with the anti-GluA1 antibody. Blots were further probed using anti-GluN2A, -2B, and -α tubulin

antibodies. Right panels: quantification of GluN2A, 2B and GluA1 levels relative to α tubulin. Results are expressed as percentage of respective Co (in (**A)**: mRNA n=5-7, proteins n=9 of each; in (**B**): n=5 of each analyzed in 3 independent experiments, ∗*P*<0.05, Mann-Whitney test).

(C) Representative Western blots of control (Co) and bexarotene (bex) treated cortical cells (n=10), hippocampal cells (n=9-10) and slices (n=5) lysates in cultures. Expression of GluA2 was monitored with the anti-GluA2 antibody. Blots were further probed using anti-α tubulin antibodies. Right panels: quantification of GluA2/α tubulin ratios. Results are expressed as percentage of respective Co analyzed in 3 independent experiments, ∗*P*<0.05, ∗∗*P*<0.01; ∗∗∗*P*<0.001, Student's *t*-test.

Data information: data are presented as mean ± SEM.

Figure S3. RXR activation increases CREB and PPARα labelling in neurons and astrocytes.

(A) Left panel: RT-qPCR analyses of *Creb1* and *Gria1* mRNA levels in control (Co, n=7-10) and 100 nM bexarotene (bex, n=10) treated primary cultures of cortical neurons for 24h (4 independent experiments analyzed). Results are expressed as percentage of respective Co (∗*P*< 0.05, ∗∗∗*P*<0.001, Student's *t*-test). Middle panel: Representative Western blot of Co and bex treated cortical cell lysates. Right panel: quantification of CREB relative to α tubulin. Results are expressed as percentage of respective Co (Co n=12, bex n=8, analyzed in 4 independent experiments, CREB: ∗∗∗*P*<0.001, Student's *t*-test). **(B**, **C)** Immunofluorescence staining of CREB (**B**) and PPARα (**C**) in Co and bex (100 nM, 24h) treated cortical cells in cultures. CREB and PPARα were labelled with the anti-CREB and anti-PPAR alpha (green) antibodies. Anti-MAP2 (blue) and -GFAP (red) antibodies were used to label neurons and astrocytes,

respectively. Scale bar, 100 µm. Higher magnification images are shown from the boxed regions; scale bar, 30 µm. White arrow: neuron; open arrow: astrocyte. CREB and PPARα signals were quantified in Co and bex treated cells. Data are normalized to Co (CREB: n=7 and PPARα: n=4 of each, analysed in 3 independent experiments, $*P<0.05$, Student's *t*-test).

Data information: data are presented as mean ± SEM.

Figure S4. Deficiency in PPARα decreases GluA1 and CREB expression and AMPA responses.

(A) PPARα expression was analyzed by semi-quantitative RT-PCR from cultured mouse cortical cells prepared from wild type (*Wt*, n=3) and *Ppara* deficient mice (*Ppara*$^{-/-}$, n=3). **(B)** Immunofluorescence staining of PPARα in *Wt* and *Ppara*$^{-/-}$ cortical cells in culture. PPARα was labelled with the anti-PPAR alpha antibody (red) in MAP2 positive neurons (blue). Scale bar, 30 µm. **(C)** RT-qPCR analyses of *Gria1* and *Creb1* mRNA levels from cultured mouse cortical cells prepared from *Wt* (n=5) and *Ppara*$^{-/-}$ (n=5). Results obtained in 3 independent experiments are expressed as percentage of corresponding *Wt* ($**P<0.01$; Mann-Whitney test). **(D)** Representative Western blots of cortical cell lysates in *Wt* and *Ppara*$^{-/-}$ cultures. Right panels: quantification of GluA1/α tubulin ratios. Results are expressed as percentage of respective *Wt* (*Wt* and *Ppara*$^{-/-}$ n=6 of each analyzed in 3 independent experiments, $***P<0.001$, Student's *t*-test). **(E)** Normalized fluorescence intensity of Fura-2 AM (Ca^{2+} indicator) in *Wt* and *Ppara*$^{-/-}$ cortical cells in presence of AMPA. Insets: amplitude of AMPA responses is expressed as ΔF/F0 (*Wt* n=163 and *Ppara*$^{-/-}$ n=121 cells analysed in 3 independent experiments, respectively; $***P<0.001$, ns: not significant, ($P>0.05$), Mann-Whitney test).

Data information: data are presented as mean ± SEM.

Figure S5. GluA1 expression and AMPA responses are decreased in AAV-ShPpara transduced cortical cells.

(A, **B)** Cortical cultures transduced with AAV containing a shRNA sequence targeting *Ppara* (AAV-ShPpara). An AAV-scramble-shRNA (AAV-ShSc) was used as a control. Cells were immunolabeled for PPARα (red) and MAP2 (blue, neuronal marker). Scale bar, 200 µm. In (**A**) PPARα quantification in AAV-ShSc or AAV-ShPpara transduced cortical cells. Data are normalized to AAV-ShSc (n=6 of each analysed in 3 independent experiments, ∗P<0.05, Mann-Whitney test). **(B)** Recordings of calcium transients in one representative GFP positive cell (green) transduced with AAV-ShSc or AAV-ShPpara (insets). Scale bar: 5 µm. **(C)** AMPA-induced calcium fluorescence in AAV-ShSc and AAV-ShPpara cortical cells. Insets: AMPA responses amplitude expressed as ΔF/F0 (AAV-ShSc n=104, AAV-ShPpara n=108 cells analyzed in 3 independent experiments, respectively; ∗∗∗P<0.001, Mann-Whitney test). **(D)** Left panel: RT-qPCR analyses of *Gria1* and *Abca1* mRNA levels in AAV-ShSc or AAV-ShPpara transduced cells (n=9 of each analyzed in 4 independent experiments). Results are expressed as percentage of respective AAV-ShSc (GluA1: ∗∗∗P<0.001, Mann-Whitney test, ABCA1: P>0.05, Student's *t*-test). Middle panel: Representative Western blot of corresponding proteins. Right panel: GluA1 and ABCA1/α tubulin ratios. Results are expressed as percentage of respective AAV-ShSc (n=6 of each analyzed in 3 independent experiments, ∗∗∗P<0.001, Student's *t*-test).

Data information: data are presented as mean ± SEM.

Figure S6. PPARα knockdown abolishes GluA1 upregulation and AMPA responses induced by RXR activation.

(A, **B)** Cortical cells transduced with an AAV containing a scramble-shRNA (AAV-ShSc) or a shRNA sequence targeting *Ppara* (AAV-ShPpara). Left panels: RT-qPCR analyses of *Gria1* and *Abca1* mRNA levels in AAV-ShSc (**A**) and AAV-ShPpara (**B**) cells treated with 100 nM bexarotene (bex) for 24h (n=5 per condition analyzed in 3 independent experiments). Results are expressed as percentage of respective untreated cells (in (**A**) GluA1: ∗*P*< 0.05, Mann-Whitney test, ABCA1: ∗∗*P*< 0.01, Student's t-test; in (**B**) GluA1: *P*>0.05, ABCA1: ∗∗*P*<0.01, Student's *t*-test). Middle panels: Representative Western blots of cell lysates from AAV-ShSc (**A**) and AAV-ShPpara (**B**) cortical cultures treated with bex. Right panels: quantification of GluA1 and ABCA1 levels/α tubulin ratios. Results are expressed as percentage of respective untreated cells (n=5 per condition analyzed in 3 independent experiments) (in (**A**) GluA1: ∗∗*P*<0.01, Mann-Whitney test, ABCA1: ∗∗∗*P*<0.001, Student's t-test; in (**B**) GluA1: *P*>0.05, ABCA1: ∗∗∗*P*<0.001, Student's *t*-test). **(C**, **D)** AAV-ShSc (**C**) and AAV-ShPpara (**D**) cells treated with bex in presence of AMPA. Insets: amplitude of AMPA response (in (**C**) AAV-ShSc n=104, AAV-ShSc+bex n=125; in (**D**) AAV-ShPpara n=108, AAV-ShPpara+bex n=189 cells analyzed in 3 independent experiments, ∗∗∗*P*<0.001, ns: not significant (*P*>0.05), Mann-Whitney test).

Data information: data are presented as mean ± SEM.

Figure S7. PPARα and GluA1 expression in male and female Tg mice.

(A) Comparative RT-qPCR analyses of *Ppara* and *Gria1* (encoding PPARα and GluA1, respectively) mRNA levels in the hippocampus from male (♂) and female (♀) 5xFAD transgenic (Tg) mice at 9-10 months old. Results were normalized to *Gapdh* mRNA and are expressed as percentage of corresponding Tg ♀ (♂ and ♀: PPARα n=5; GluA1 n=6 of each, ∗*P*<0.05, ∗∗*P*<0.01; Student's *t* test). PPARα expression were visualized by semi-quantitative RT-PCR

(right panel). **(B)** Representative Western blot of hippocampal lysates from female (♀) and male (♂) Tg mice. Expression of GluA1 was monitored with the anti-GluA1 antibody and blots were further probed using anti-α tubulin antibody. Right panel: quantification of GluA1/α tubulin ratios. Results are expressed as percentage of Tg ♀ (n=4 for each condition, $**P<0.01$, Student's *t* test). **(C)** CA1 LTP in hippocampal slices from male (♂) transgenic (Tg) 5xFAD mice (9-10 mo) perfused with 4 µM bexarotene (bex, n=4) or with vehicle (veh, n=2), *** P<0.001, Student's t test.

Data information: data are presented as mean ± SEM.

Figure S8. **PDK4 expression is induced in Tg mice by pemafibrate although a decrease in PPARs is observed.**

(A) Comparative RT-qPCR analyses of *Pdk4* mRNA levels in the hippocampus of transgenic (Tg) 5xFAD mice treated at 12 months old with the PPARα agonist pemafibrate (pema) (1 mg/kg/day, Tg + pema, n=12) or vehicle (Tg + veh, n=8) (water 0.1% Tween 80, Tg + veh) by gavage (12 days). Results were normalized to *Gapdh* mRNA and are expressed as percentage of Tg + veh ($**P<0.01$, Student's *t* test). **(B)** Comparative RT-qPCR analyses of *Ppara*, *Pparb* and *Pparg* (encoding PPARα, PPARβ and PPARγ, respectively) mRNA levels in the hippocampus of transgenic (Tg) 5xFAD and age-matched control non-transgenic wild type (Wt) mice at 9-10 months old (n=4 of each). Results were normalized to *Gapdh* mRNA and are expressed as percentage of corresponding non-Tg ($**P<0.01$, $*P<0.05$, Student's *t* test).

Data information: data are presented as mean ± SEM.

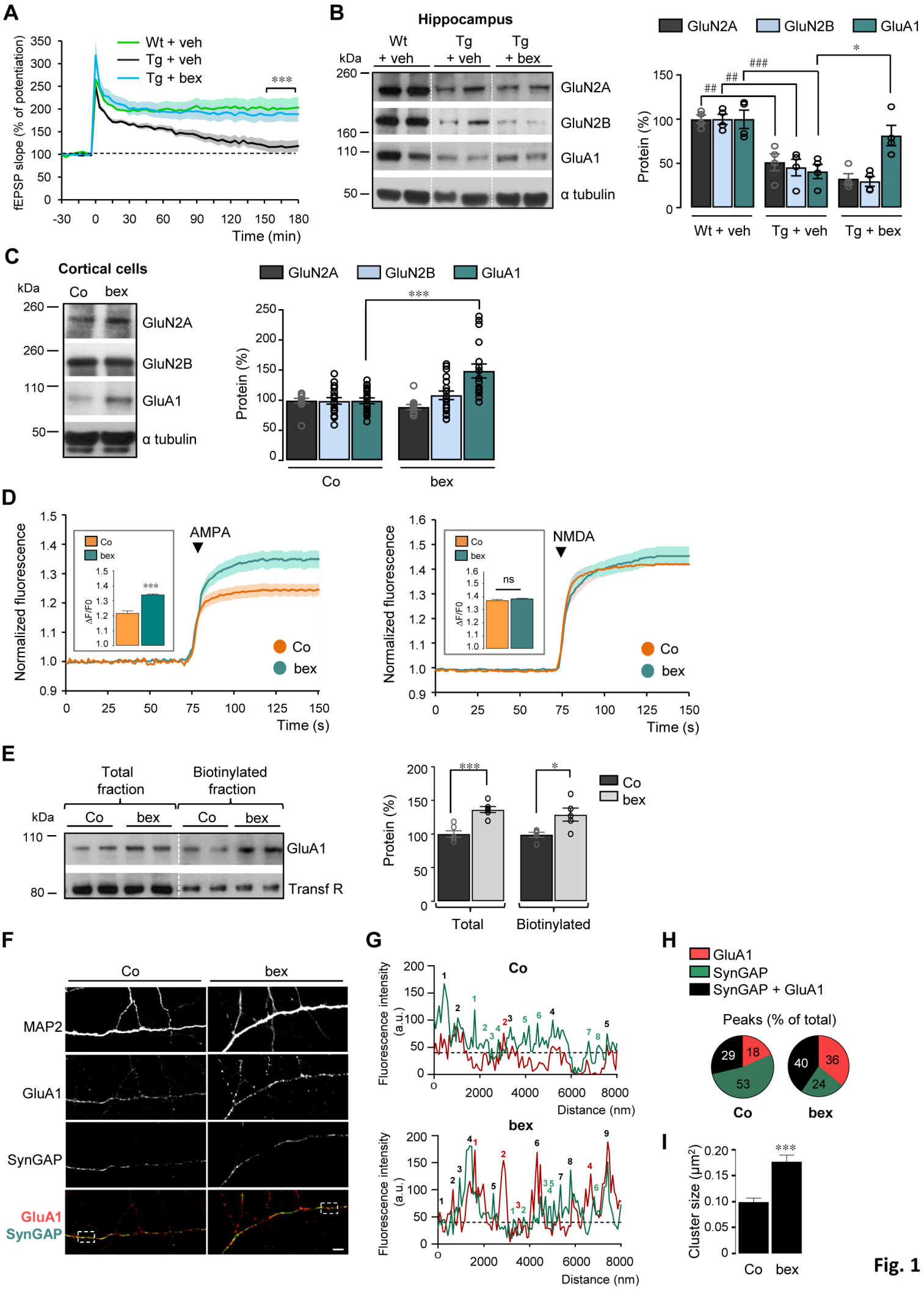
A
Wt + veh
Tg + veh
Tg + bex
***
fEPSP slope (% of potentiation)
Time (min)
B
Hippocampus
Wt + veh
Tg + veh
Tg + bex
kDa
GluN2A
GluN2B
GluA1
α tubulin
GluN2A
GluN2B
GluA1
Protein (%)
##
##
###
*
Wt + veh
Tg + veh
Tg + bex
C
Cortical cells
Co
bex
GluN2A
GluN2B
GluA1
α tubulin
***
Protein (%)
Co
bex
D
AMPA
NMDA
Normalized fluorescence
Time (s)
Co
bex
***
ns
ΔF/F0
E
Total fraction
Biotinylated fraction
Co
bex
GluA1
Transf R
Protein (%)
***
*
Total
Biotinylated
F
Co
bex
MAP2
GluA1
SynGAP
GluA1
SynGAP
G
Co
bex
Fluorescence intensity (a.u.)
Distance (nm)
H
GluA1
SynGAP
SynGAP + GluA1
Peaks (% of total)
29
18
53
40
36
24
Co
bex
I
Cluster size (μm²)
***
Co
bex

Fig. 1

Fig. 2

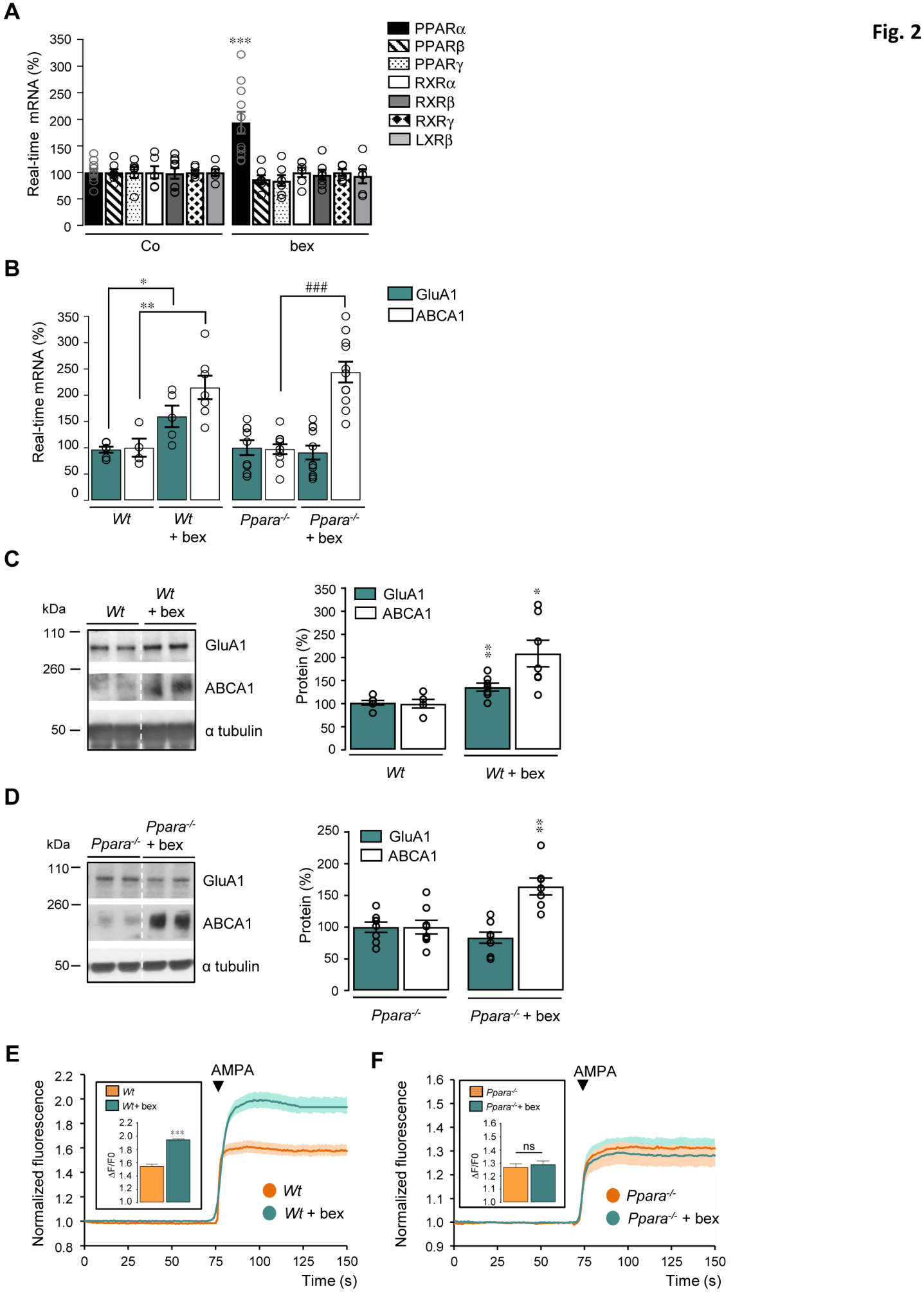
A
PPARα
PPARβ
PPARγ
RXRα
RXRβ
RXRγ
LXRβ
Real-time mRNA (%)
Co
bex
B
GluA1
ABCA1
Real-time mRNA (%)
Wt
Wt + bex
Ppara-/-
Ppara-/- + bex
C
kDa
Wt
Wt + bex
110
260
50
GluA1
ABCA1
α tubulin
Protein (%)
D
Ppara-/-
Ppara-/- + bex
E
AMPA
Wt
Wt + bex
Normalized fluorescence
Time (s)
F
Ppara-/-
Ppara-/- + bex
ns

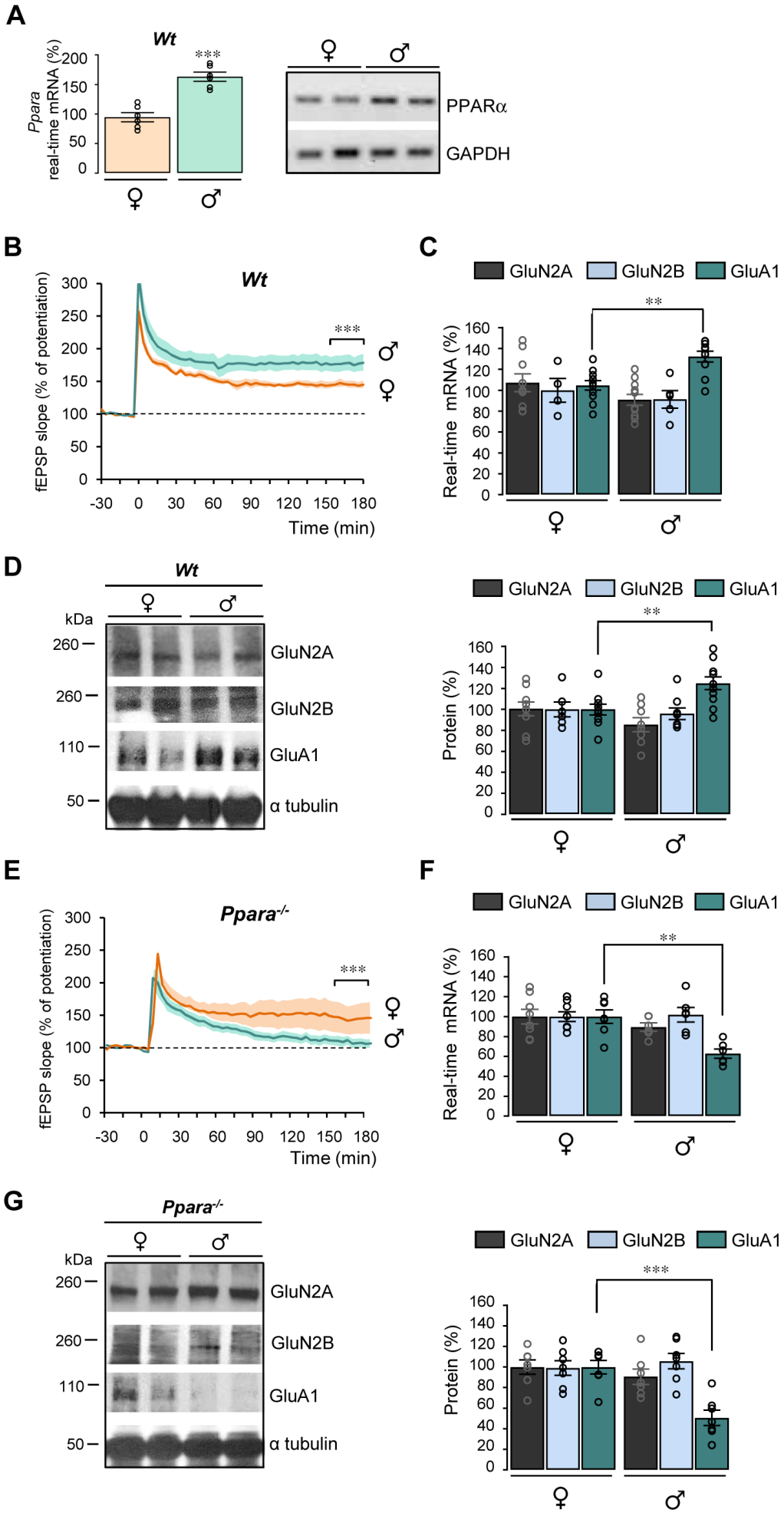
A
Wt
Ppara real-time mRNA (%)
200
150
100
50
0
***
♀
♂
PPARα
GAPDH
B
Wt
fEPSP slope (% of potentiation)
300
250
200
150
100
50
0
***
-30
0
30
60
90
120
150
180
Time (min)
C
GluN2A
GluN2B
GluA1
**
Real-time mRNA (%)
160
140
120
100
80
60
40
20
0
D
Wt
kDa
260
260
110
50
GluN2A
GluN2B
GluA1
α tubulin
Protein (%)
E
Ppara-/-
F
G
Ppara-/-

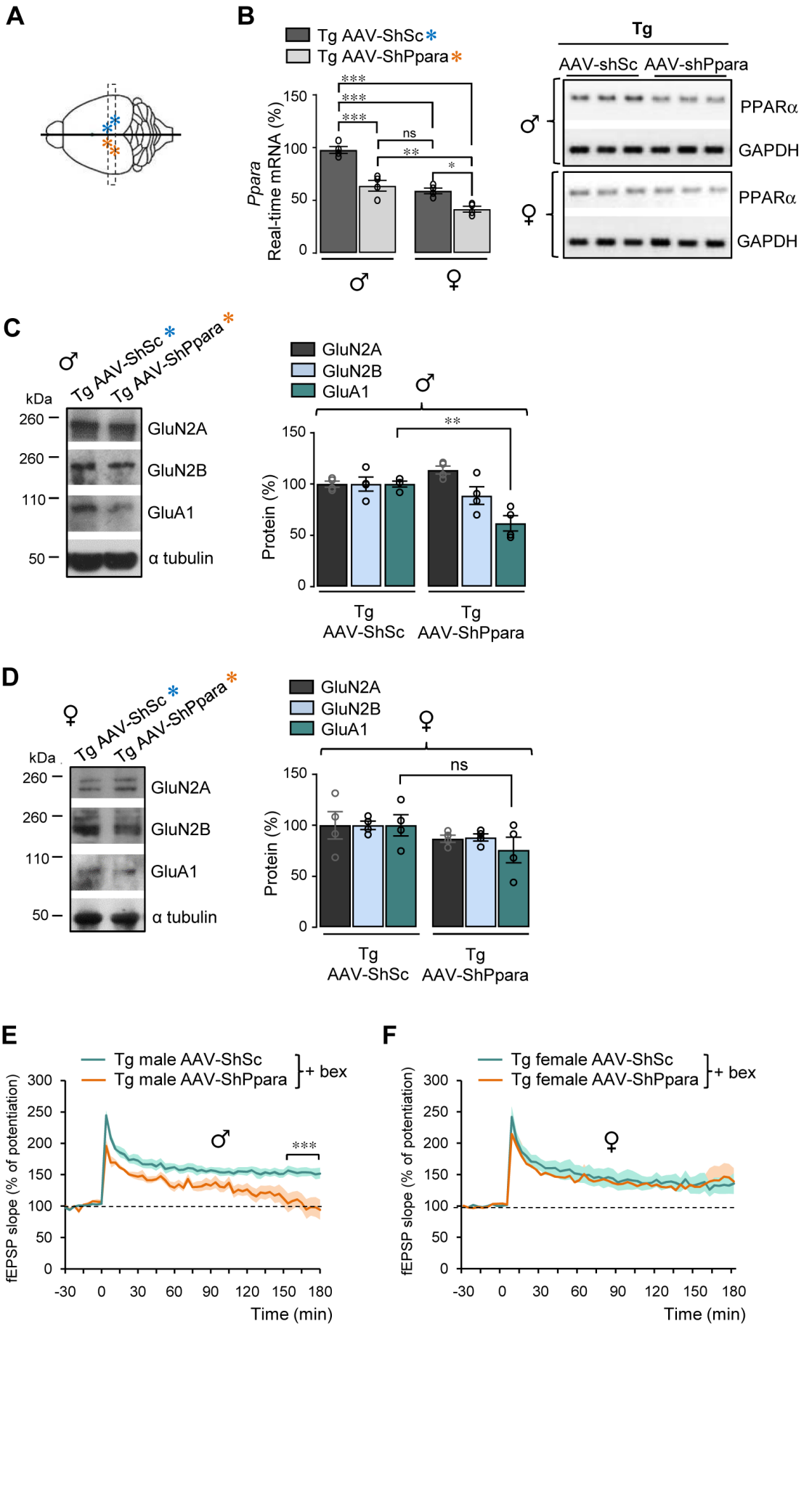
A
B
Tg AAV-ShSc
Tg AAV-ShPpara
Ppara Real-time mRNA (%)
150
100
50
0
***
***
***
ns
**
*
♂
♀
Tg
AAV-shSc
AAV-shPpara
PPARα
GAPDH
PPARα
GAPDH
C
♂
Tg AAV-ShSc
Tg AAV-ShPpara
kDa
260
260
110
50
GluN2A
GluN2B
GluA1
α tubulin
GluN2A
GluN2B
GluA1
♂
**
Protein (%)
150
100
50
0
Tg
AAV-ShSc
Tg
AAV-ShPpara
D
♀
Tg AAV-ShSc
Tg AAV-ShPpara
kDa
260
260
110
50
GluN2A
GluN2B
GluA1
α tubulin
GluN2A
GluN2B
GluA1
♀
ns
Protein (%)
150
100
50
0
Tg
AAV-ShSc
Tg
AAV-ShPpara
E
Tg male AAV-ShSc
Tg male AAV-ShPpara
+ bex
♂
***
fEPSP slope (% of potentiation)
300
250
200
150
100
50
0
-30
0
30
60
90
120
150
180
Time (min)
F
Tg female AAV-ShSc
Tg female AAV-ShPpara
+ bex
♀
fEPSP slope (% of potentiation)
300
250
200
150
100
50
0
-30
0
30
60
90
120
150
180
Time (min)

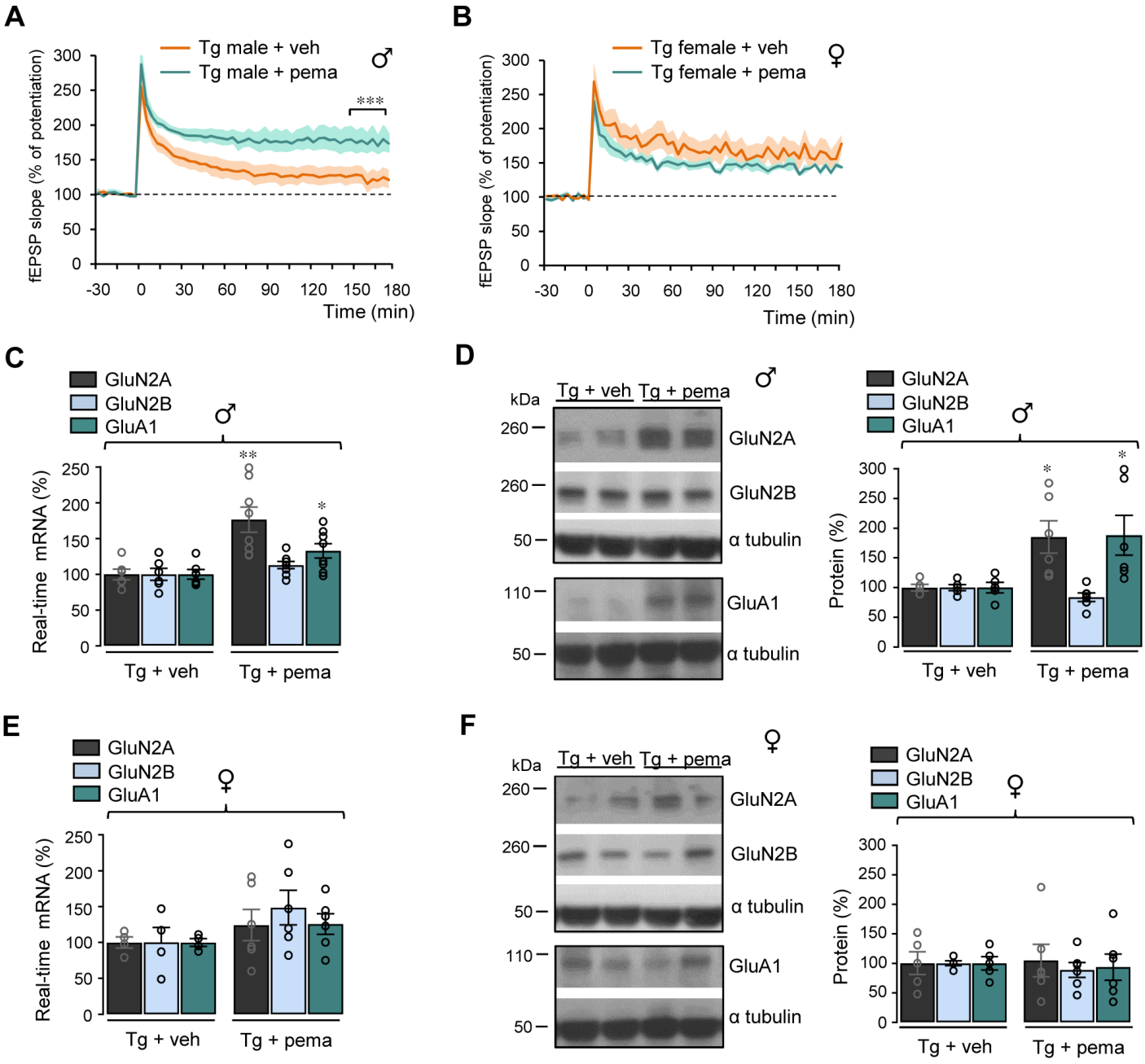
A
Tg male + veh
Tg male + pema
♂
***
fEPSP slope (% of potentiation)
Time (min)
B
Tg female + veh
Tg female + pema
♀
fEPSP slope (% of potentiation)
Time (min)
C
GluN2A
GluN2B
GluA1
♂
Real-time mRNA (%)
Tg + veh
Tg + pema
D
kDa
Tg + veh
Tg + pema
♂
GluN2A
GluN2B
α tubulin
GluA1
α tubulin
GluN2A
GluN2B
GluA1
♂
Protein (%)
Tg + veh
Tg + pema
E
GluN2A
GluN2B
GluA1
♀
Real-time mRNA (%)
Tg + veh
Tg + pema
F
kDa
Tg + veh
Tg + pema
♀
GluN2A
GluN2B
α tubulin
GluA1
α tubulin
GluN2A
GluN2B
GluA1
♀
Protein (%)
Tg + veh
Tg + pema

A

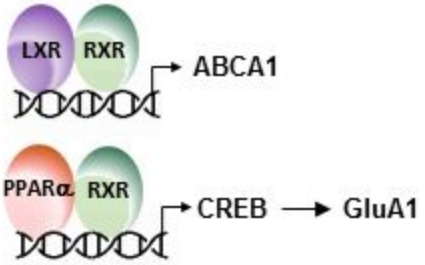

B

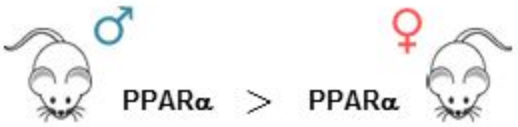

PPARα > PPARα

GluA1 > GluA1

Synaptic plasticity > Synaptic plasticity

Figure S1

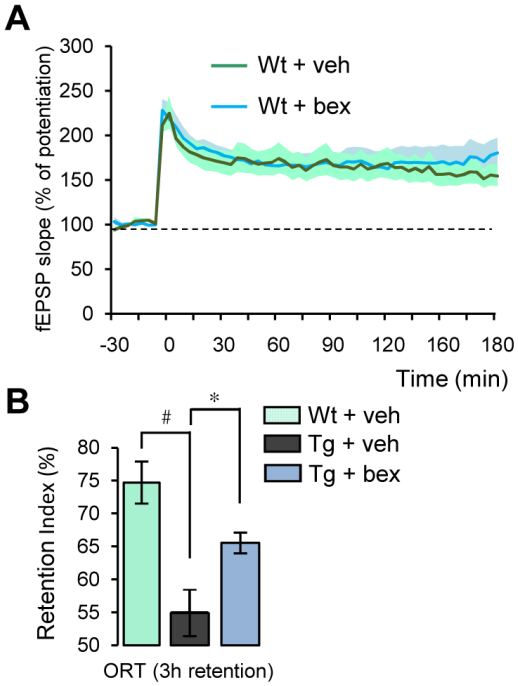
A
Wt + veh
Wt + bex
fEPSP slope (% of potentiation)
300
250
200
150
100
50
0
-30
0
30
60
90
120
160
180
Time (min)

B
#
*
Wt + veh
Tg + veh
Tg + bex
Retention Index (%)
80
75
70
65
60
55
50
ORT (3h retention)

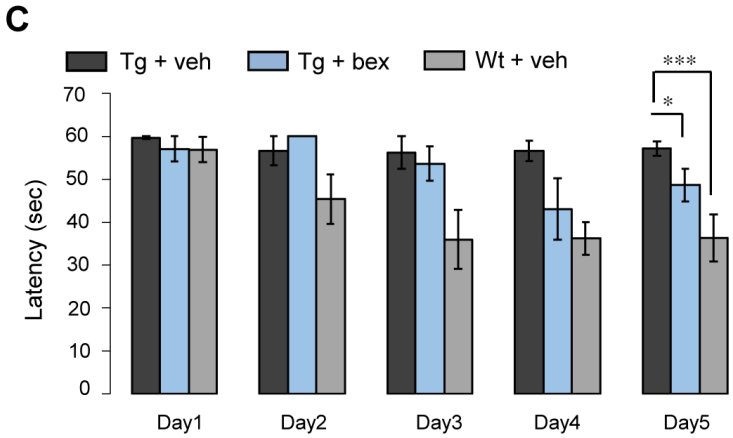
C
Tg + veh
Tg + bex
Wt + veh
***
*
Latency (sec)
70
60
50
40
30
20
10
0
Day1
Day2
Day3
Day4
Day5

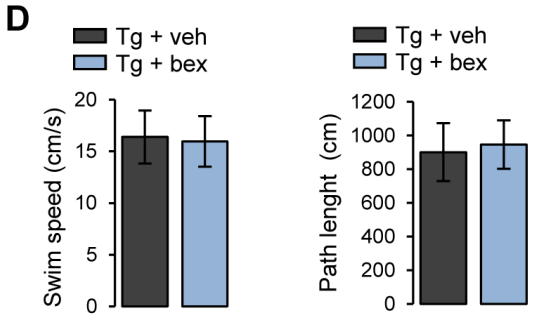
D
Tg + veh
Tg + bex
Swim speed (cm/s)
20
15
10
5
0
Tg + veh
Tg + bex
Path lenght (cm)
1200
1000
800
600
400
200
0

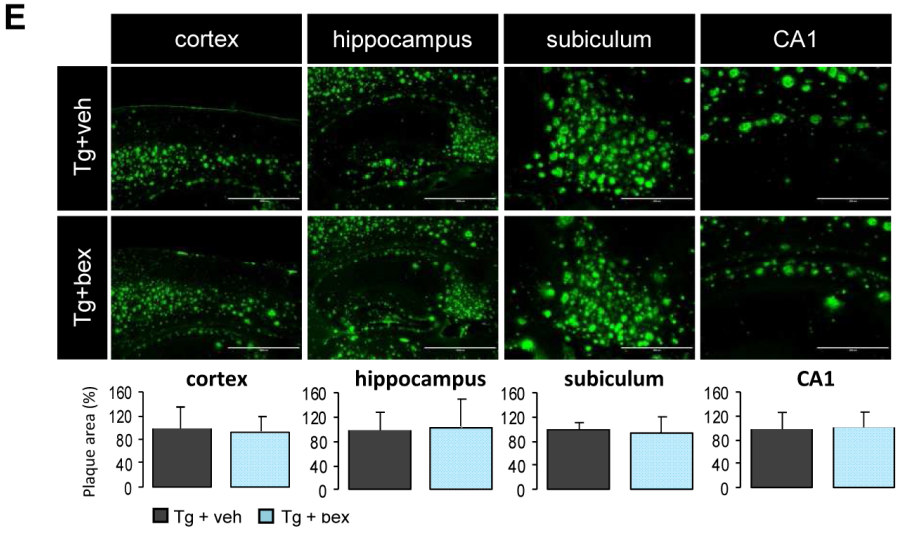
E
cortex
hippocampus
subiculum
CA1
Tg+veh
Tg+bex
cortex
hippocampus
subiculum
CA1
Plaque area (%)
160
120
80
40
0
Tg + veh
Tg + bex

Figure S2

A

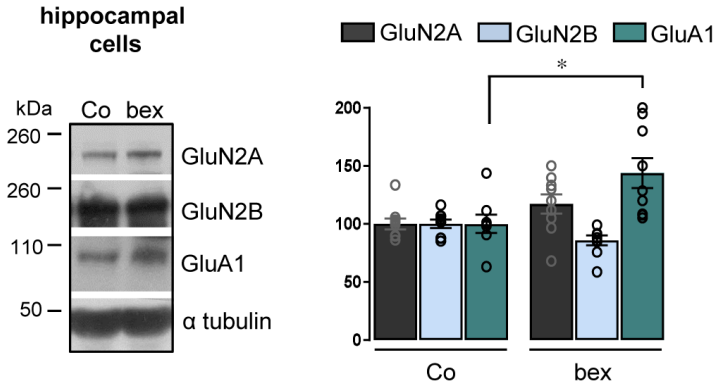

B

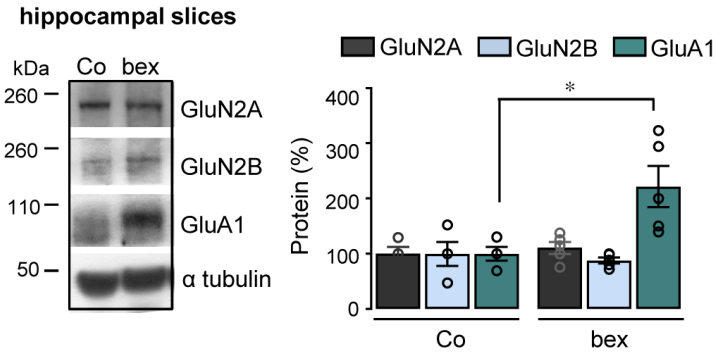

C

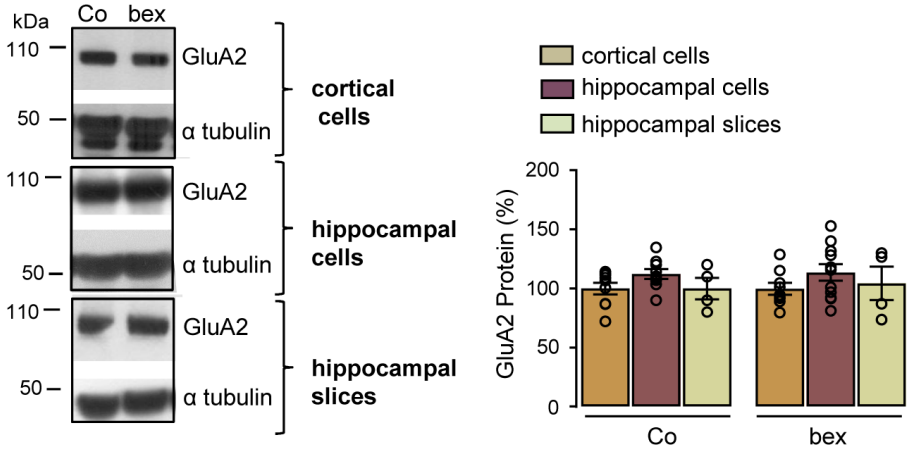

Figure S3

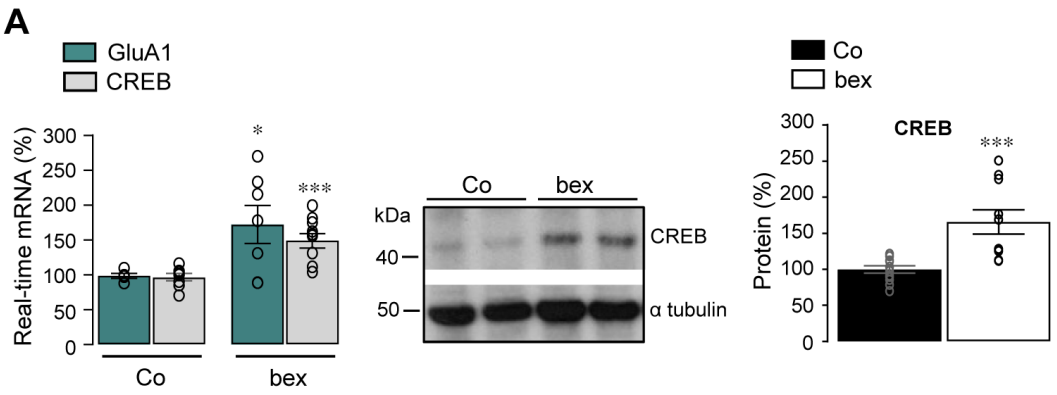
A
GluA1
CREB
Real-time mRNA (%)
300
250
200
150
100
50
0
*
***
Co
bex
kDa
40
50
CREB
α tubulin
Co
bex
CREB
***
Protein (%)
300
250
200
150
100
50
0

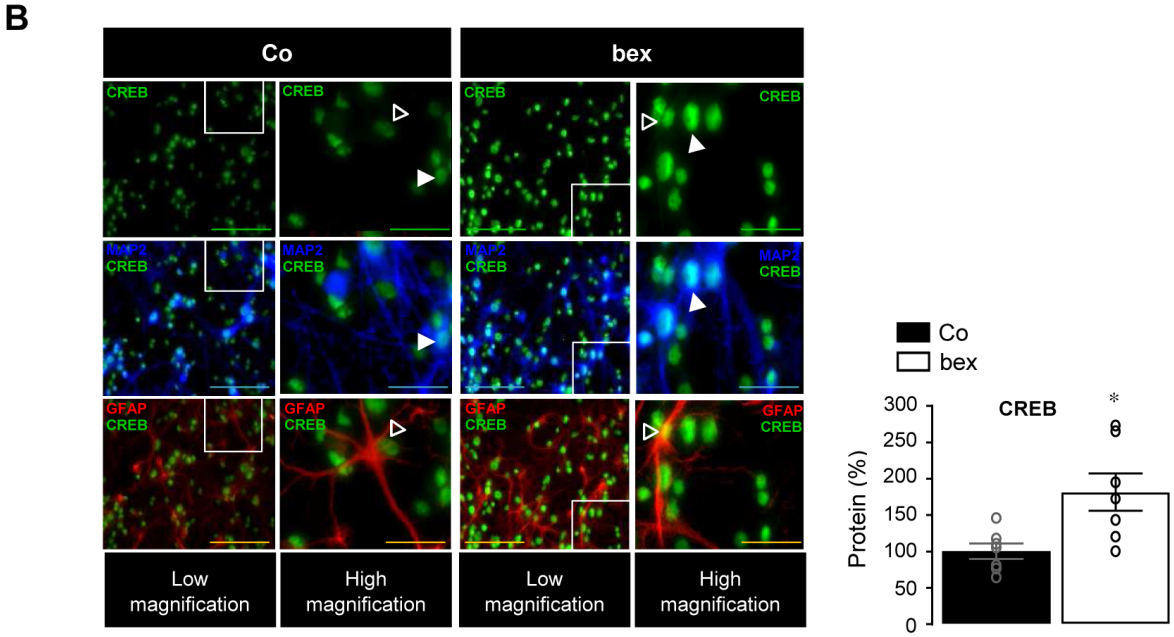
B
Co
bex
CREB
MAP2
GFAP
Low magnification
High magnification
Low magnification
High magnification
Co
bex
CREB
Protein (%)
300
250
200
150
100
50
0
*

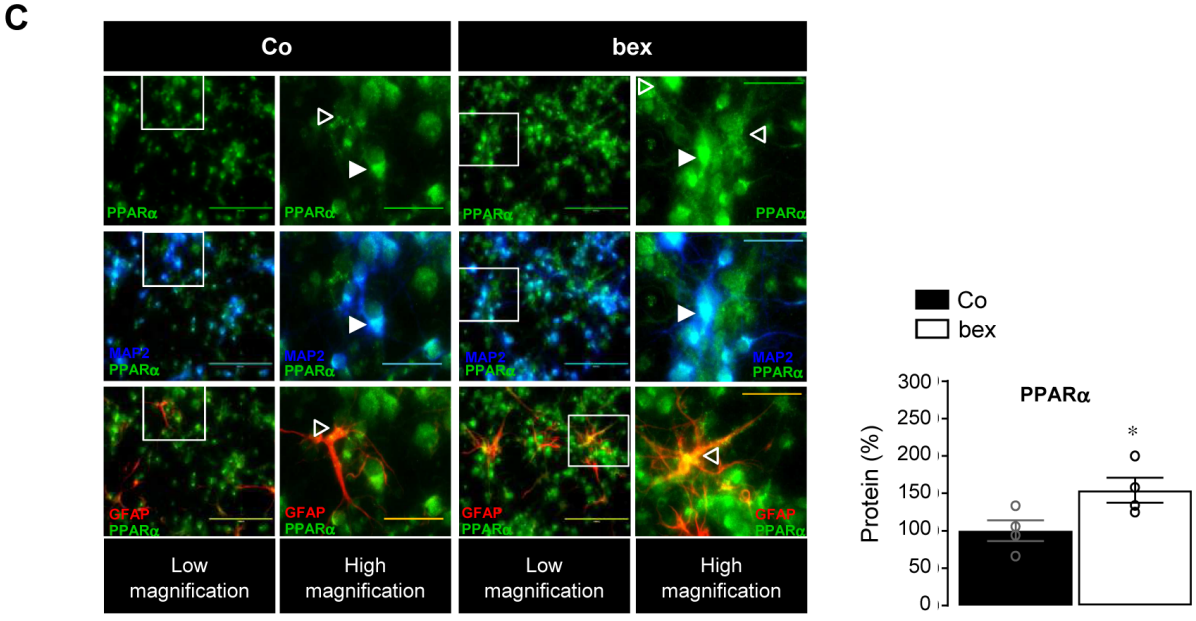
C
Co
bex
PPARα
MAP2
GFAP
Low magnification
High magnification
Low magnification
High magnification
Co
bex
PPARα
Protein (%)
300
250
200
150
100
50
0
*

Figure S4

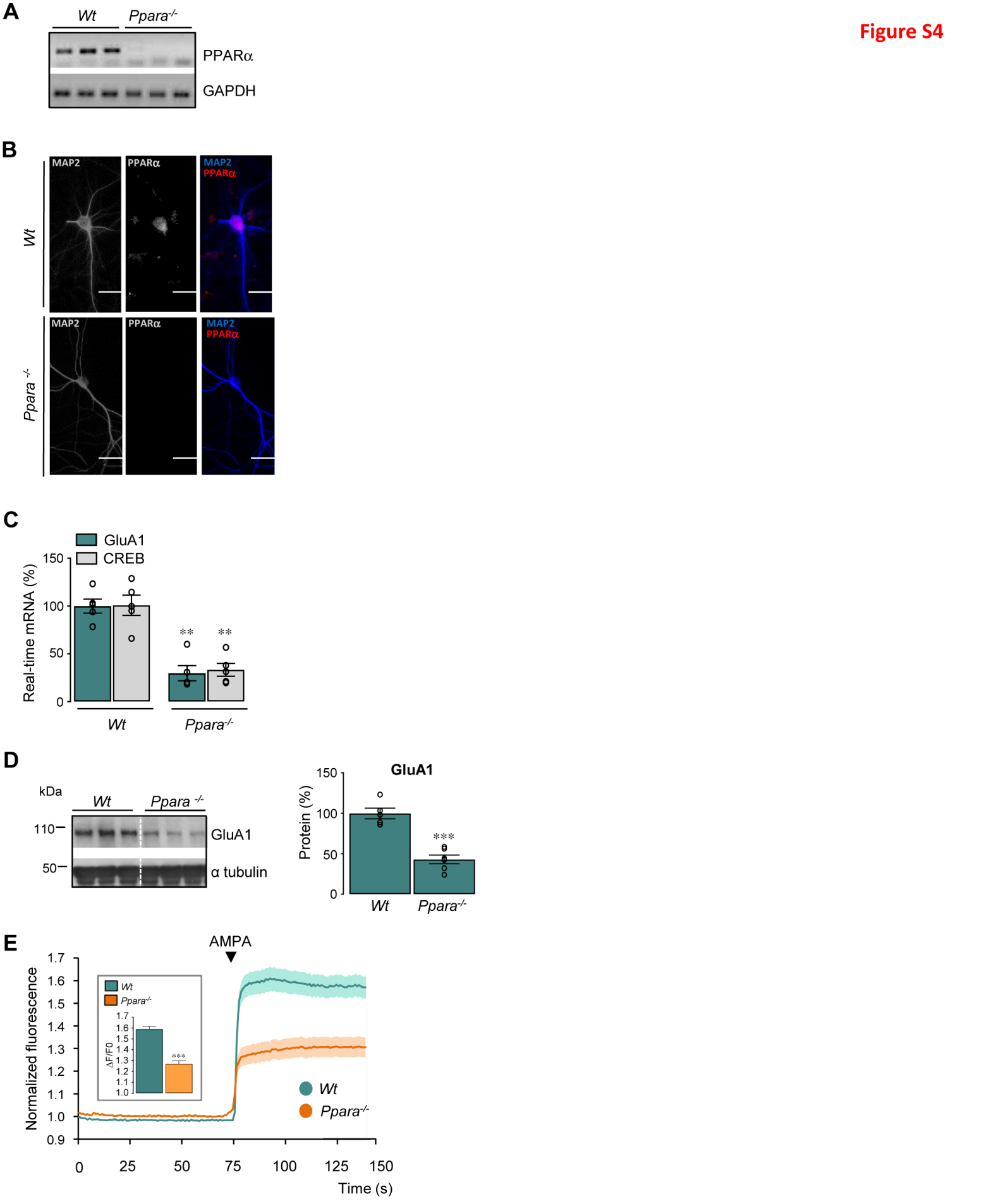
A
Wt
Ppara-/-
PPARα
GAPDH
B
MAP2
PPARα
MAP2
PPARα
Wt
MAP2
PPARα
MAP2
PPARα
Ppara -/-
C
GluA1
CREB
Real-time mRNA (%)
150
100
50
0
**
**
Wt
Ppara-/-
D
kDa
Wt
Ppara -/-
110
50
GluA1
α tubulin
GluA1
Protein (%)
150
100
50
0
***
Wt
Ppara-/-
E
AMPA
Normalized fluorescence
1.7
1.6
1.5
1.4
1.3
1.2
1.1
1.0
0.9
Wt
Ppara-/-
ΔF/F0
***
Wt
Ppara-/-
0
25
50
75
100
125
150
Time (s)

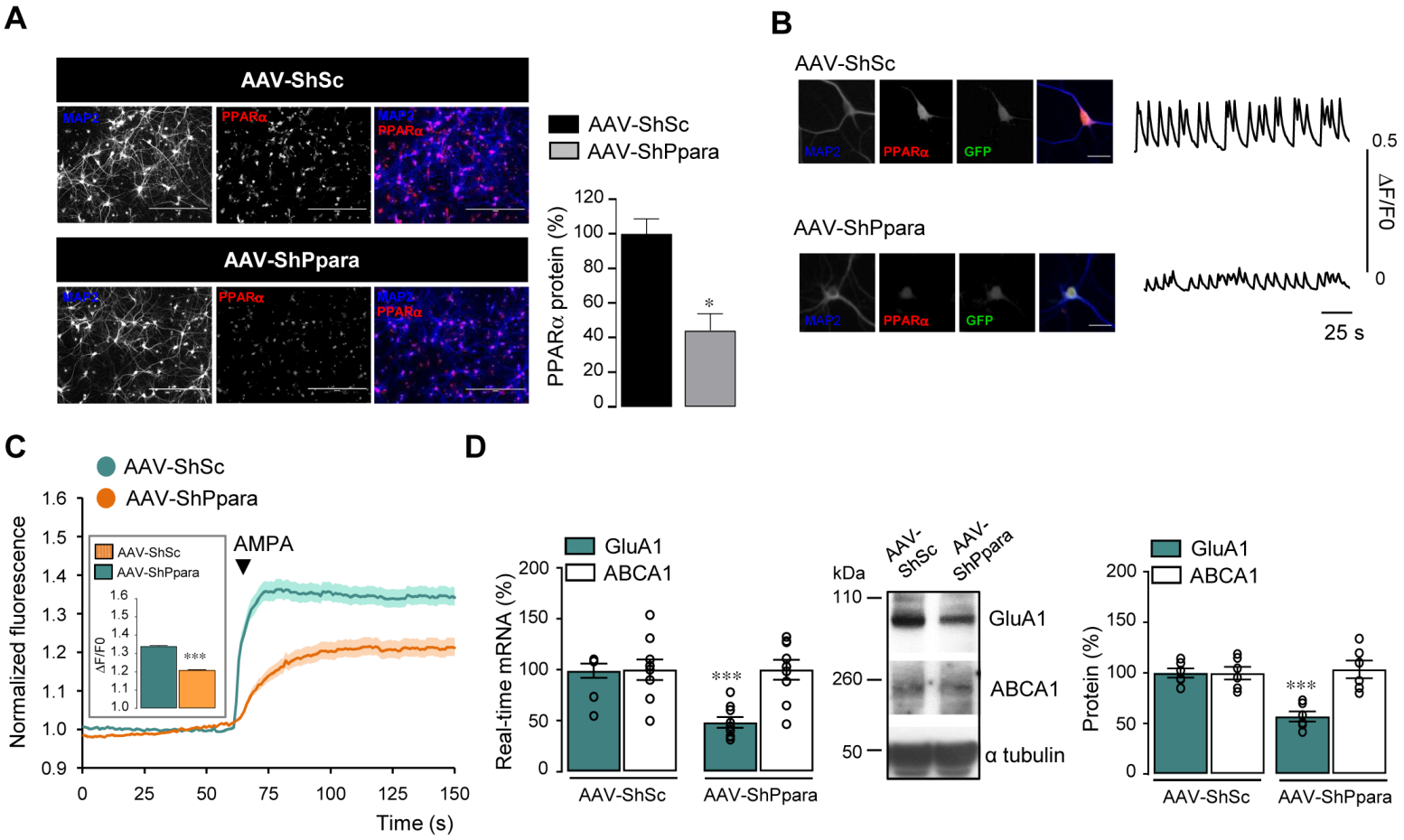
A
AAV-ShSc
MAP2
PPARα
AAV-ShPpara
AAV-ShSc
AAV-ShPpara
PPARα protein (%)
B
AAV-ShSc
AAV-ShPpara
GFP
ΔF/F0
25 s
C
AAV-ShSc
AAV-ShPpara
AMPA
Normalized fluorescence
Time (s)
D
GluA1
ABCA1
Real-time mRNA (%)
kDa
α tubulin
Protein (%)

Figure S5

Figure S6

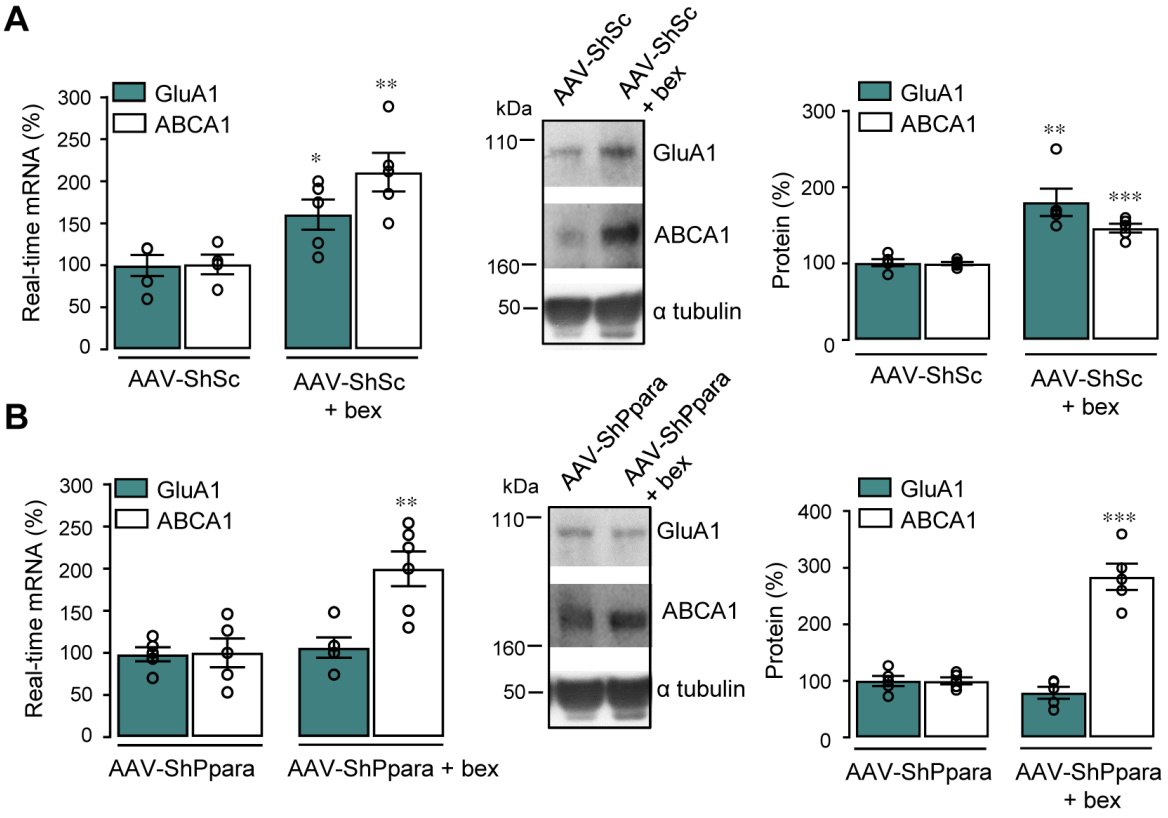
A
GluA1
ABCA1
Real-time mRNA (%)
AAV-ShSc
AAV-ShSc + bex
kDa
110
160
50
GluA1
ABCA1
α tubulin
Protein (%)
B
AAV-ShPpara
AAV-ShPpara + bex

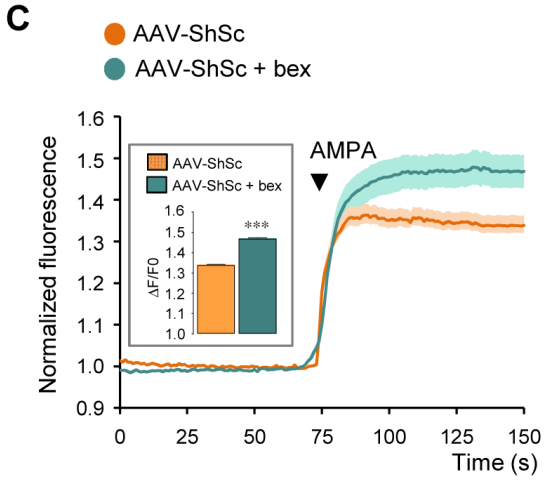
C
AAV-ShSc
AAV-ShSc + bex
AMPA
Normalized fluorescence
ΔF/F0
***
Time (s)

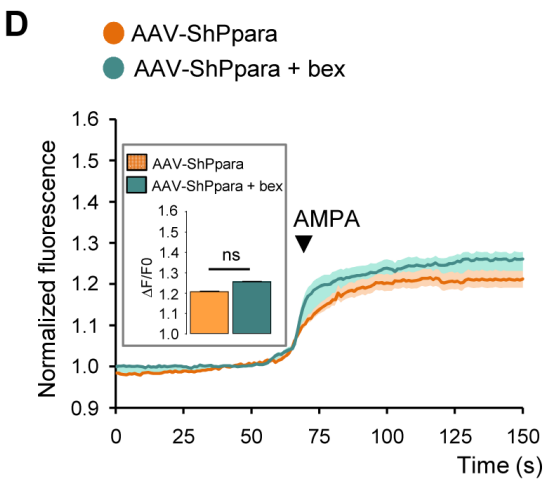
D
AAV-ShPpara
AAV-ShPpara + bex
AMPA
Normalized fluorescence
ΔF/F0
ns
Time (s)

Figure S7

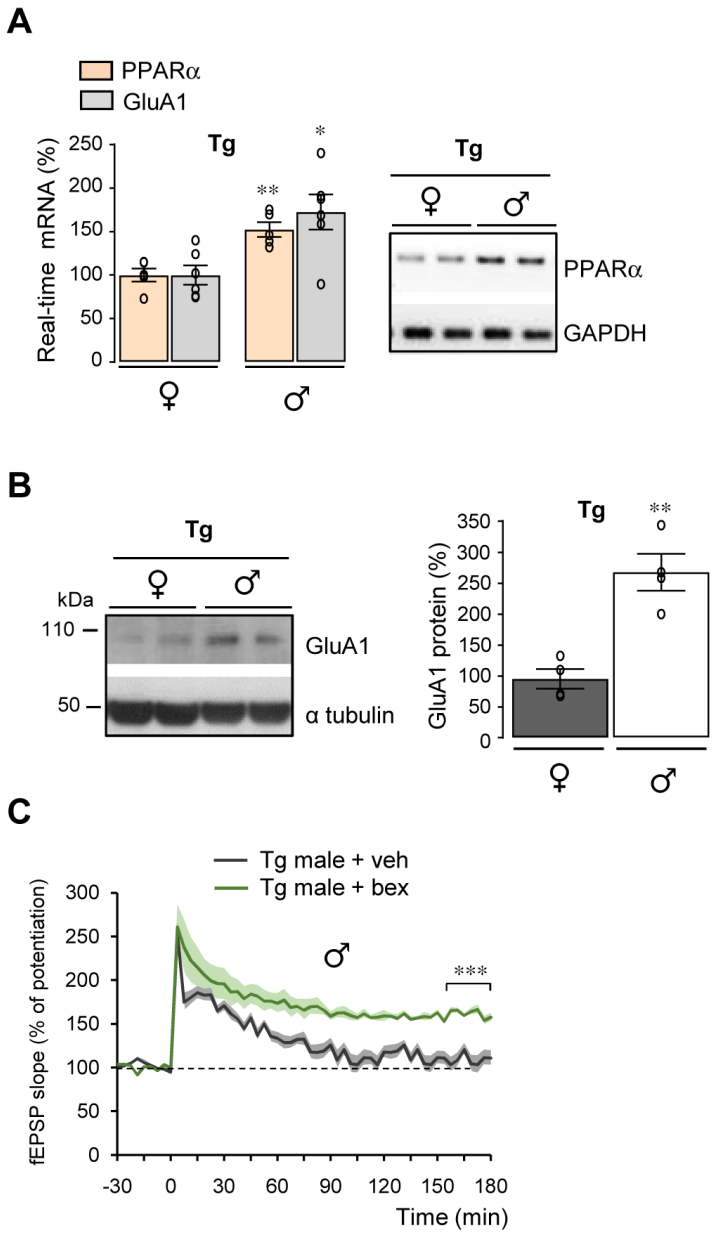
A
PPARα
GluA1
Tg
Real-time mRNA (%)
250
200
150
100
50
0
**
*
♀
♂
Tg
♀
♂
PPARα
GAPDH
B
Tg
♀
♂
kDa
110
50
GluA1
α tubulin
Tg
**
GluA1 protein (%)
350
300
250
200
150
100
50
0
♀
♂
C
Tg male + veh
Tg male + bex
fEPSP slope (% of potentiation)
300
250
200
150
100
50
0
♂
***
-30
0
30
60
90
120
150
180
Time (min)

Figure S8

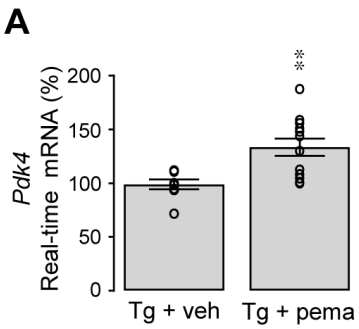
A
Pdk4
Real-time mRNA (%)
200
150
100
50
0
Tg + veh
Tg + pema

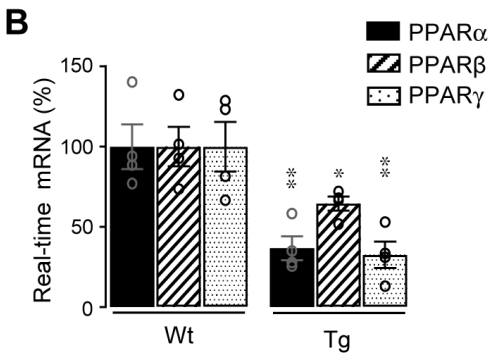
B
PPARα
PPARβ
PPARγ
Real-time mRNA (%)
150
100
50
0
Wt
Tg